

**CONSTRAINT ON DARK MATTER CENTRAL DENSITY IN
THE EDDINGTON INSPIRED BORN-INFELD (EiBI)
GRAVITY WITH INPUT FROM WEYL GRAVITY**

Alexander A. Potapov^{1,a}, Ramil Izmailov^{2,b}, Olga Mikolaychuk^{1,c},
Nikolay Mikolaychuk^{1,c}, Mithun Ghosh^{3,d} and Kamal K. Nandi^{1,2,3,e}

¹Department of Physics & Astronomy, Bashkir State University,
Sterlitamak Campus, Sterlitamak 453103, RB, Russia

²Zel'dovich International Center for Astrophysics, M. Akmullah Bashkir
State Pedagogical University, Ufa 450000, RB, Russia

³Department of Mathematics, University of North Bengal, Siliguri 734013,
WB, India

^aEmail: potapovaa@mail.ru

^bEmail: izmailov.ramil@gmail.com

^cEmail: mikov94@mail.ru

^dEmail: ghoshmithun123@gmail.com

^eEmail: kamalnandi1952@yahoo.co.in

PACS number(s): 04.50.Kd, 95.30.Sf, 04.50.1h

Abstract

Recently, Harko *et al.* (2014) derived an approximate metric of the galactic halo in the Eddington inspired Born-Infeld (EiBI) gravity. In this metric, we show that there is an upper limit ρ_0^{upper} on the central density ρ_0 of dark matter such that stable circular orbits are possible *only* when the constraint $\rho_0 \leq \rho_0^{\text{upper}}$ is satisfied in each galactic sample. To quantify different ρ_0^{upper} for different samples, we follow the novel approach of Edery & Paranjape (1998), where we use as input the geometric halo radius R_{WR} from Weyl gravity and equate it with the dark matter radius R_{DM} from EiBI gravity for the same halo boundary. This input then shows that the known fitted values of ρ_0 obey the constraint $\rho_0 \leq \rho_0^{\text{upper}} \propto (R_{\text{WR}})^{-2}$. Using the mass-to-light ratios giving α , we shall also evaluate $\rho_0^{\text{lower}} \propto (\alpha - 1)M_{\text{lum}}R_{\text{WR}}^{-3}$ and the average dark matter density $\langle \rho \rangle^{\text{lower}}$. Quantitatively, it turns out that the interval $\rho_0^{\text{lower}} \leq \rho_0 \leq \rho_0^{\text{upper}}$ verifies reasonably well against many dark matter dominated low surface brightness (LSB) galaxies for which values of ρ_0 are independently known. The interval holds also in the case of Milky

Way galaxy. Qualitatively, the existence of a stability induced upper limit ρ_0^{upper} is a remarkable prediction of the EiBI theory.

Key Words: Dark matter, central density, modified gravity

I. INTRODUCTION

Early observations [1-3] on rotational data of spiral galaxies, now reconfirmed by observations extending well beyond the optical disc [4-18], indicate that they do not conform to Newtonian gravity predictions. Hence the hypothesis is that there could be large amounts of non-luminous matter hidden in the galactic haloes. The rationale is this: Doppler emissions from stable circular orbits of neutral hydrogen clouds in the halo allow measurement of tangential velocity v_{tg} of the clouds treated as probe particles. Contrary to Newton's laws, where v_{tg}^2 should decay with radius r , observations indicate that it approximately levels off with r in the galactic halo region, which in turn calls for the presence of additional non-luminous mass, the so called dark matter. Since dark matter has not yet been directly observed, the dark matter hypothesis is often variantly referred to as the missing mass problem.

Several well known theoretical models for dark matter exist in the literature but it is impossible to list all of them here (only some are mentioned in [19-34]). In its usual formulation, dark matter is a parametrization of the observed velocity discrepancies and is not a prediction of the formulation. Some simulations require fine tuning of halo parameters to luminous parameters galaxy by galaxy – a procedure that only enlarges the number of parameters rather than reducing them (See [35], pp.32-33; see also footnote 13). There exist yet another variety of halo models, which treat the missing mass problem as a failure of the Newtonian theory on galactic distance scales rather than as a prediction for dark matter. Such models actually do *not* require dark matter at all for the interpretation of observed rotation data. This class of theories include, e.g., Modified Newtonian Dynamics (MOND) developed by Milgrom [36-42], Scalar-Tensor-Vector Gravity theory developed by Moffat [43-45], Weyl conformal gravity¹ implemented by Mannheim and O'Brien [48]. For brevity, we call the last the MO model and we shall use this ingredient in the sequel. A remarkable speciality of the MO model is that, using the best available galactic optical and radio data, and a standardized, non-biased, treatment for selecting appropriate galactic

¹Weyl conformal gravity has been debated for and against in the literature. For instance, Flanagan [46] argues that if the source has associated with it a macroscopic long range scalar field, breaking conformal symmetry, the theory does not reproduce attractive gravity in the solar system. However, subsequently, Mannheim [47] has counter-argued that Schwarzschild tests of solar gravity could still be recovered even in the presence of such macroscopic fields.

parameters, the model is able to provide a good fit to the rotation curves *without* the need for any dark matter whatsoever.

There are various other (non-)dark matter models that are capable of accounting, for example, for observations of galaxy clusters and gravitational lensing or structure formation. A leading example is the cold dark matter (CDM) model, which is a part of the current standard model Λ CDM of cosmology. These models are based on different phenomenologies such as inflation and nucleosynthesis [49-66]. They can successfully explain observations of galaxy clusters [49-54], gravitational lensing [55,56] or structure formation [57], to name the most important ones. These models postulate that galactic cores may consist of axions [58], massive gravitons [59], BEC [60] or other collisionless particles. The post-recombination fluctuation spectrum nicely explains the formation of galaxies and clusters [49-54]. The CDM is a successful paradigm accounting for the small density inhomogeneities that seed structure formations 10^{-34} sec after the bang and as such provides a bold probe into the Early Universe [57]. Some other and recent works on CDM models are mentioned here though the list by no means is exhaustive [61-66].

Recently, another alternative candidate for dark matter is also being speculated. This is based on the evidence of soft positron spectrum in the AMS-02 [67,68] cosmic ray data. Despite this alternative, the observed flat rotation curves are still considered as a robust proof that dark matter essentially is of gravitational origin described by general relativity [69-71]. But in general relativity, matter-gravity coupling is linear, while some authors argue (for non-minimal coupling of modified gravity with matter or other insights into the paradigm, see [72-77]) that there is no obvious reason as to why the coupling should be linear. Following this thought, an interesting modification of matter-gravity coupling leading to the Eddington-inspired Born-Infeld (EiBI) theory has been recently developed by Bañados and Ferreira [78,79], which we shall use as another ingredient. Only in vacuum, the EiBI theory is equivalent to standard general relativity. This new, and more general, theory has led to interesting observable predictions in the context of solar interior dynamics, big bang nucleosynthesis, neutron stars, the structure of other compact stars [80-83] including the possibility of nonsingular cosmological models and alternative to inflation [84].

To get a more complete view of the two ingredients of the present work, the EiBI and the Weyl gravity, it is necessary to mention that several important predictions follow from the two theories. For instance, recent investigation by Du *et al.* [85] on large scale structure formation in the EiBI gravity shows a deviation in the matter power spectrum between the EiBI gravity and the Λ CDM model, which is a testable prediction. Stability and localization of gravitational fluctuations in the EiBI brane system have been studied in Refs. [86,87]. Further, as shown by Wei *et al.* [88], strong gravitational lensing observables in EiBI are controlled by the coupling parameter

κ , which is a new prediction that lends itself to future testing. Similarly, in Weyl gravity, the first order light deflection angle θ_W by a galaxy, first obtained by Edery and Paranjape [89], contains the galactic halo parameter γ appearing in the MO model. Bhattacharya *et al.* [90,91] calculated higher order deflection terms. Strong field lensing in the Weyl gravity has been studied recently in [92], and the predictions can be verified by actual observations in future. A remarkable feature of Weyl gravity is that its solution, the MO model, already contains the successes of the well tested Schwarzschild gravity as a special case. All the above exemplify the current status of the capabilities of the two theories in question.

The possibility of perfect fluid dark matter within the framework of general relativity has already been explored in the literature [93,94]. A similar possibility has been recently investigated within the framework of the EiBI theory by Harko *et al.* [95,96] and this is the model we are going to analyze further in this paper. Using a tangential velocity profile [97,98] giving Universal Rotation Curves (URC) and setting the cosmological constant to zero, they obtained, in the Newtonian approximation, a new galactic metric and theoretically explored its gravitational properties. However, the numerical values of the crucial parameter κ (denoted by $\kappa = 2R_{\text{DM}}^2/\pi^2$) or equivalently the dark matter radius R_{DM} , cannot be determined from the theory alone – it has to be obtained either from the observed data or from some other model.² It is also expected that the values of R_{DM} would differ from galaxy to galaxy. On the other hand, to our knowledge, apart from the observed last scattering radii R_{last} , the astrophysical literature still seems to lack concrete observed data on R_{DM} for individual galaxies. Therefore, an appropriate numerical input for R_{DM} is needed, which we take from Weyl gravity, if we want to make *quantitative* predictions.

At this point, we recall a novel idea of Edery & Paranjape [89], where they bridged two different metric theories by equating the *same* Einstein angle θ_E (caused by the luminous + dark matter) with the Weyl angle θ_W (caused by the luminous matter alone), and drew useful and testable conclusions using the identity $\theta_E = \theta_W$. Motivated exactly by this idea, we equate the *same* EiBI radius of dark matter R_{DM} (caused by dark matter source) with the geometric Weyl radius of the galactic halo R_{WR} (caused by the luminous matter alone). With the numerical input $R_{\text{DM}} = R_{\text{WR}}$, we shall quantify the relevant central densities in the EiBI theory (see footnote 8). *We wish to clarify that we are not talking here of merging or mapping the two theories into one another per se but concentrating only on a particular*

²We wish to clarify that the EiBI parameter κ is not a universal constant – it's more like a parameter of the theory that assumes different values depending on the physical situation. For instance, the structure of compact general relativistic star requires a value $\kappa \simeq 10^{12} \text{ cm}^2$ [82], which differs from the value $\kappa \simeq 10^{44} \text{ cm}^2$ inferred from dark matter density profiles.

common prediction. The theories are of course different from each other – one with dark matter source and the other without, not to mention differences elsewhere. But both are metric theories capable of predicting for *any* given galactic sample a dark matter/halo boundary arising out of the same stability condition $V'' < 0$ (as used, e.g., in the braneworld dark matter [99]). Therefore, without any bias to either theories, we shall investigate if this input leads to limits on dark matter central density ρ_0 consistent with those estimated from fits to different known profiles. We shall see that it does.

The radius R_{WR} is to be understood as the geometric halo radius with its interior being filled with Weyl vacuum.³ We stress that Weyl vacuum is *not* a vacuum in the ordinary sense but an arena of interplay of several potential energies, predominantly the global quadratic potential due to cosmic inhomogeneities [48]. Thus, our input physically means that the total potential energy contained within the halo radius R_{WR} of Weyl gravity equals the total invisible dark matter energy contained within R_{DM} of EiBI gravity. The radius R_{DM} is defined by the absence of dark matter density at the halo boundary [95,96], while R_{WR} is defined by the absence of stable circular orbits at the halo boundary [100]. Since stability is an essential physical criterion because Doppler emissions from the halo emanate from stable circular orbits of hydrogen gas [101], we think that R_{WR} should be regarded as the only testable upper limit on the radius of a galactic halo. Fortunately, observed last scattering data R_{last} so far have not surpassed the predicted limiting value R_{WR} for all the galaxies studied to date, thereby lending excellent observational support to the MO model prediction of R_{WR} .

The purpose of the present paper is as follows: We shall concentrate on the low surface brightness (LSB) galaxies that are mostly dominated by dark matter. We show that there is an upper limit on the dark matter central density ρ_0 specific to each individual galaxy, which we call here ρ_0^{upper} , such that stable circular orbits in the EiBI are possible *only* when the constraint $\rho_0 \leq \rho_0^{\text{upper}} \propto (R_{\text{WR}})^{-2}$ is satisfied in that galaxy. Using the Weyl gravity input $R_{\text{DM}} = R_{\text{WR}}$, we shall then quantify ρ_0^{upper} , and show that the central density ρ_0 predicted from the fit to various simulations including the NFW and Burkert density profiles does obey the constraint. Taking into account the range of the rather uncertain but possible mass-to-light ratios (denoted, say, by α), we shall calculate also the lower central density $\rho_0^{\text{lower}} \propto (\alpha - 1)M_{\text{lum}}R_{\text{WR}}^{-3}$ and find that $\rho_0^{\text{lower}} \leq \rho_0 \leq \rho_0^{\text{upper}}$ holds for some known LSB samples for which ρ_0 is known from independent fits. Some illustrative galactic samples including the Milky Way are tabulated. The values fall within the predicted interval for each individual galaxy and we conjecture that at least the upper limit might be generally true.

³Note that we are using here the terminology R_{WR} in lieu of $R_{\text{stable}}^{\text{max}}$ of Ref.[100] only to bring it in line with the notation of the present analysis.

The contents are organized as follows: Since both the models under consideration are relatively new, hence possibly unfamiliar, we provide in Sec.II, a brief outline of the algorithms underlying the EiBI and MO metric models of the galactic halo. In Sec.III, we shall graphically explore ρ_0^{upper} for stability of circular orbits in EiBI. In Sec.IV, using the input under consideration, we shall quantify upper and lower central densities for some samples to see if the estimated central densities ρ_0 truly fall within the proposed interval, that is, if $\rho_0^{\text{lower}} \leq \rho_0 \leq \rho_0^{\text{upper}}$. In Sec.V, we discuss the dark matter density profiles in the context of Milky Way. The results are summarized in Sec.VI. We shall take units such that $8\pi G = 1$, $c = 1$, unless restored.

II (a): EiBI MODEL

For easy reference, we outline only the salient features of the EiBI dark matter model developed in [95,96]. The EiBI action is [78,79,85,102,103]

$$S_{\text{EiBI}} = \frac{2}{\kappa} \int d^4x \left[\sqrt{-|g_{\mu\nu} + \kappa R_{\mu\nu}(\Gamma)|} - \lambda \sqrt{-|g_{\mu\nu}|} \right] + S_{\text{matter}}, \quad (1)$$

where λ is a dimensionless parameter, $g_{\mu\nu}$ is the physical metric, $R_{\mu\nu}(\Gamma)$ is the symmetric part of the Ricci tensor built solely from the connection $\Gamma_{\beta\gamma}^\alpha$ ($\equiv \frac{1}{2}q^{\alpha\sigma} [\partial_\gamma q_{\sigma\beta} + \partial_\beta q_{\sigma\gamma} - \partial_\sigma q_{\beta\gamma}]$) derived from an auxiliary metric denoted by $q_{\mu\nu}$. The meaning of the auxiliary metric $q_{\mu\nu}$ is that it partially satisfies Eddington field equations so that $2\kappa\sqrt{|R|}R^{\mu\nu} = \sqrt{|q|}q^{\mu\nu}$, which can be rewritten as Einstein field equations if we equate $q_{\mu\nu}$ with $g_{\mu\nu}$ and κ with Λ^{-1} . For small values of κR , the action (1) reproduces the Einstein-Hilbert action with $\lambda = \kappa\Lambda + 1$, where Λ is the cosmological constant, while for large values of κR , the action approximates to that of Eddington, viz., $S_{\text{Edd}} = 2\kappa \int d^4x \sqrt{|R|}$. For more details, see [78,79].

Harko *et al.* [95,96] deals with dark matter modeling assuming certain restrictive conditions such as spherical symmetry and asymptotic flatness, the latter requiring that $\Lambda = 0 \Leftrightarrow \lambda = 1$. These assumptions of course limit the applicability of EiBI theory but makes the problem at hand much simpler to handle. One spin-off is that the description of the physical behavior of various cosmological and stellar scenarios was assumed to be controlled by the only remaining parameter κ . The galactic halo is assumed to be filled with perfect fluid dark matter with energy-momentum tensor $T^{\mu\nu} = pg^{\mu\nu} + (p + \rho)U^\mu U^\nu$, $g_{\mu\nu}U^\mu U^\nu = -1$ and the tangential velocity profile provided by the Universal Rotation Curve (URC) [97,98]

$$v_{\text{tg}}^2 = v_\infty^2 \frac{(r/r_{\text{opt}})^2}{(r/r_{\text{opt}})^2 + r_0^2}, \quad (2)$$

where r_{opt} is the optical radius containing 83% of the galactic luminosity, r_0 is the halo core radius in units of r_{opt} , the asymptotic velocity $v_\infty^2 =$

$v_{\text{opt}}^2(1 - \beta_*)(1 + r_0^2)$, $v_{\text{opt}} = v_{\text{tg}}(r_{\text{opt}})$, $\beta_* = 0.72 + 0.44\text{Log}_{10}(L/L_*)$, $L_* = 10^{10.4}L_{\odot}$. For spiral galaxies, $r_0 = 1.5(L/L_*)^{1/5}$. Under the Newtonian approximations that the pressure $p \simeq 0$, $8\pi\kappa\rho \ll 1$, and $(r/r_{\text{opt}})^2 \gg r_0^2$, the EiBI field equations yield the Lane-Emden equation with polytropic index $n = 1$, which has an exact nonsingular solution for dark matter density distribution as [95,96] ⁴

$$\rho^{(0)}(r) = \rho_0 \left[\frac{\sin\left(r\sqrt{\frac{2}{\kappa}}\right)}{r\sqrt{\frac{2}{\kappa}}} \right], \quad (3)$$

where $\rho^{(0)}(0) = \rho_0$ is the constant central density. Assuming that the halo has a sharp boundary R_{DM} , where the density vanishes such that $\rho^{(0)}(R_{\text{DM}}) = 0$, one has

$$R_{\text{DM}} = \pi\sqrt{\frac{\kappa}{2}}. \quad (4)$$

The density profile (3) exhibits an unphysical behavior of becoming negative for $R_{\text{DM}} < R < 2R_{\text{DM}}$, which is why one has to require a sharp halo boundary $\rho^{(0)}(R \geq R_{\text{DM}}) = 0$.⁵ This quite specific behavior of the density profile differs from those of Navarro-Frenk-White (NFW) or Burkert density profiles (that decay to zero only as $r \rightarrow \infty$).⁶

The mass profile of the dark matter is

$$M(r) = 4\pi \int_0^r \rho^{(0)}(r)r^2 dr = \frac{4R_{\text{DM}}^3}{\pi^2} \rho_0 [\sin(\bar{r}) - \bar{r} \cos(\bar{r})], \quad (5)$$

where the dimensionless quantity $\bar{r} = \pi r/R_{\text{DM}}$. The total mass of the dark matter M_{DM} and the mean density $\langle \rho \rangle$ in EiBI theory are given respectively by

$$M_{\text{DM}} = M(R_{\text{DM}}) = \frac{4}{\pi} \rho_0 R_{\text{DM}}^3, \quad \langle \rho \rangle = \frac{3\rho_0}{\pi^2}. \quad (6)$$

The approximate physical metric has been derived in [35] as⁷

$$d\tau^2 = -B(\bar{r})dt^2 + A(\bar{r})d\bar{r}^2 + \bar{r}^2 C(\bar{r})(d\theta^2 + \sin^2\theta d\phi^2), \quad (7)$$

⁴The solution (3) to the Lane-Emden equation and its connection to dark matter was first pointed out in [96].

⁵We thank an anonymous referee for pointing this out.

⁶The observational situation is that the mass density profiles on the logarithmic scale clearly indicate that the density is decaying at a finite radius [104]. While NFW or Burkert density profiles might lead to different physical metrics of interest, the key point of the present investigation is that the dark matter has a finite radius following from *stability* considerations [100]. See also footnote 11.

⁷The role of the URC profile (2) is that it determines the metric function $B(r) [\equiv e^{\nu(r)}]$. Following Chandrasekhar [105], we know that the tangential velocity is given by $v_{\text{tg}}^2 = \frac{r}{2e^{\nu}}(e^{\nu})_{,r}$. See the details in Ref.[93]. Using the URC for v_{tg}^2 , defining $r/r_{\text{opt}} = x$, and integrating, we obtain $e^{\nu(r)} = (x^2 + r_0^2)v_{\infty}^2$. Restoring the original variable r/r_{opt} , and defining $\bar{r} = \pi r/R_{\text{DM}}$, we immediately obtain the metric function $B(\bar{r})$ of Eq.(8).

$$B(\bar{r}) = e^{\nu_0} \left[\left(\frac{R_{\text{DM}}}{\pi r_{\text{opt}}} \right)^2 \bar{r}^2 + r_0^2 \right]^{v_\infty^2}, \quad (8)$$

$$A(\bar{r}) = \left(\frac{R_{\text{DM}}}{\pi} \right)^2 \frac{1}{\left[1 - \frac{\bar{\rho}_0}{\bar{r}} \sin(\bar{r}) + \bar{\rho}_0 \cos(\bar{r}) \right] \left[1 - \frac{\bar{\rho}_0}{\bar{r}} \sin(\bar{r}) \right]}, \quad (9)$$

$$C(\bar{r}) = \left(\frac{R_{\text{DM}}}{\pi} \right)^2 \left[1 - \frac{\bar{\rho}_0}{\bar{r}} \sin(\bar{r}) \right], \quad (10)$$

where e^{ν_0} is an arbitrary constant of integration (which we set to unity) and the dimensionless quantity $\bar{\rho}_0 = \frac{8\rho_0 R_{\text{DM}}^2}{\pi}$.

Note that the surface area of a sphere at the boundary of dark matter halo defined by $\bar{r} = \pi$, has the value $S = 4\pi\bar{r}^2 C(\bar{r}) = 4\pi\bar{r}^2 \left(\frac{R_{\text{DM}}}{\pi} \right)^2 = 4\pi R_{\text{DM}}^2$, which is just the spherical surface area in "standard coordinates". Thus the dark matter radius R_{DM} can be identified with standard coordinate halo radius R_{HR} derived below. We shall need some of the above equations in the sequel.

II (b): MANNHEIM-O'BRIEN MODEL

The unique Weyl action is

$$\begin{aligned} S_{\text{Weyl}} &= -\alpha_g \int d^4x \sqrt{-g} \left[C_{\lambda\mu\nu\sigma} C^{\lambda\mu\nu\sigma} \right] \\ &= -2\alpha_g \int d^4x \sqrt{-g} \left[R_{\mu\sigma} R^{\mu\sigma} - \frac{1}{3} (R_\alpha^\alpha)^2 \right], \end{aligned} \quad (11)$$

where $C^{\lambda\mu\nu\sigma}$ is the Weyl tensor and α_g is the dimensionless gravitational constant. The resulting field equations are fourth order and trace free, rather long and complicated, so we omit them here. The exact solution of vacuum Weyl gravity for the metric ansatz

$$d\tau^2 = -B(r)dt^2 + \frac{1}{B(r)}dr^2 + r^2(d\theta^2 + \sin^2\theta d\phi^2) \quad (12)$$

was derived by Mannheim & Kazanas [43] that describes the metric outside of a localized static, spherically symmetric source of radius r_0 embedded in a region with $T_{\mu\nu}(r > r_0) = 0$ as follows (after suitably redefining the constants):

$$B(r) = (1 - 6M\gamma)^{1/2} - \frac{2M}{r} + \gamma r - kr^2, \quad (13)$$

where M, γ, k are constants of integration. Schwarzschild solution is recovered at $\gamma = 0, k = 0$ as a special case of Weyl gravity.

On the other hand, in Refs.[48,107], the arguments and calculations instead proceed from the considerations of *potential*. In Weyl gravity, a given

local gravitational source generates a gravitational potential per unit solar mass as follows (Eq.(8) of Ref.[107]):

$$V^* = -\frac{\beta^* c^2}{r} + \frac{\gamma^* c^2 r}{2},$$

where β^* and γ^* are constants. Then, on integrating V^* over the local luminous matter distribution, one obtains the local contribution to tangential velocity at $r = R > 4R_0$ [107]:

$$\frac{v_{\text{loc}}^2}{R} \simeq \frac{N^* \beta^* c^2}{R^2} \left(1 - \frac{9R_0^2}{2R^2}\right) + \frac{N^* \gamma^* c^2}{2} \left(1 - \frac{3R_0^2}{2R^2} - \frac{45R_0^4}{8R^4}\right). \quad (14)$$

The meanings and values of the symbols above are as follows: R_0 is the scale length such that most of the surface brightness is contained in $R \leq 4R_0$ of the optical disk region, N^* is total number of solar mass units in the luminous galaxy obtained via the mass-to-light ratio: $(M/L)L = M_{\text{lum}} = N^* M_{\odot}$. Thereafter, detailed arguments (See Refs.[48,107]) are used to introduce two additional potentials of *cosmological* origin, viz., $\frac{\gamma_0 c^2 R}{2}$ and $-kc^2 R^2$, that contribute to velocity such that

$$\frac{v_{\text{tg}}^2}{R} = \frac{v_{\text{loc}}^2}{R} + \frac{\gamma_0 c^2}{2} - kc^2 R. \quad (15)$$

The numerical values of the constants giving best fits to rotation curves of all the 111 galaxy samples in [107] are:

$$\begin{aligned} \beta^* &= GM_{\odot}/c^2 = 1.48 \times 10^5 \text{ cm}, \quad \gamma^* = 5.42 \times 10^{-41} \text{ cm}^{-1}, \\ \gamma_0 &= 3.06 \times 10^{-30} \text{ cm}^{-1}, \quad k = 9.54 \times 10^{-54} \text{ cm}^{-2}. \end{aligned} \quad (16)$$

It is evident from Eq.(15) that, in making the fits, the *only* parameter that can vary from one galaxy to the other is the mass-to-light ratio (M/L) leading to a galaxy dependent N^* . The mass of HI gas is known and included in the fit. With everything else being universal, no hypothetical dark matter is needed – potential effects of cosmological origin plus the local potential caused by the luminous mass of a galaxy are enough to account for the observed rotation data.

For each galaxy with specific value of N^* and other fixed constants as in (16), v_{tg}^2 of Eq.(15) gives a *finite* value of R at the terminating velocity $v_{\text{tg}}^2(R_{\text{term}}) = 0$, where the potentials balance. To illustrate various results derived here, we need to consider samples and so in the following we choose the LSB galactic sample ESO 1200211. The reason for this choice is that it is one of the samples, whose central dark matter density has been recently fitted to various known density profiles by Robles & Matos [108] and thus it lends itself to easy comparison with the results of the present paper. The

plot in Fig.1 shows that the rotation curve v_{tg}^2 decays to zero at a radial distance $R_{\text{term}} = 52.04$ kpc, but this is still not the halo radius! The actual halo radius R_{WR} , defined by the stability inequality (21) below, will always be less than the value of R_{term} for reasons of stability, as will soon be worked out.⁸

The MO prescription for v_{tg}^2 in Eq.(15) leads to the Mannheim-Kazanas metric (13) of Weyl gravity in the limit of large distances away from the galactic core in which we are interested. It can be seen as follows. The geodesic for a single test particle yields the tangential velocity of material circular orbits at the arbitrary radius $r = R$ as [107]

$$v_{\text{tg}}^2 = (Rc^2/2) B',$$

where prime denotes derivative with respect to R . Integrating, we obtain

$$B(R) = 1 - \frac{2N^*\beta^*}{R} + (N^*\gamma^* + \gamma_0) R - kR^2 + \frac{3R_0^2 N^*\gamma^*}{2R} + \frac{15R_0^4 N^*\gamma^* - 24R_0^2 N^*\beta^*}{8R^3}. \quad (17)$$

⁸Note that there are two specific profiles used in the paper: One is the URC velocity profile in Eq.(2) that is never zero at any radius, $v_{\text{tg}}^2|_{\text{URC}} \neq 0$, while the other is the MO velocity profile, Eq.(15), that can become zero at a finite radius $r = R_{\text{term}}$ such that $v_{\text{tg}}^2|_{\text{MO}}(R_{\text{term}}) = 0$. Such different behavior might call into question the validity of the identification $R_{\text{DM}} = R_{\text{WR}}$ used as an input in this paper.

The physical meaning of this input is explained on p.4. Here we point out some additional grounds justifying the input. Note that it is quite logical that two different theories can predict the *same* measurable quantity, say, light deflection. Similarly, despite differences in the behavior, the profiles still provide fitted values of the same quantity ρ_0 . Ideally, the values should exactly be the same, which is not the case, but they are comparable at least by order of magnitudes. In the present case, it is the assumed equality of the radii R_{DM} and R_{WR} provided by the two profiles that is in question. We have equated them on the ground that, observationally, there has to be only one dark matter radius for each sample, no matter how it is defined. So the equality in a way suggests itself. The other ground is that we have been motivated by the approach originally proposed by Edery & Paranjape [89], where they equated the Einstein and Weyl angles. Actually, such identifications are justified only *a posteriori*, when they are found to yield results that are independently known to be true. For instance, using the input $\theta_E = \theta_W$ for the deflection of light by galaxies, Edery & Paranjape [89] obtained the value of γ in the metric (18) that is reasonably close to that obtained independently in [48,107] by rotational data fits to samples. On the other hand, we also know that Weyl and Einstein theories, giving respectively θ_W and θ_E , are very different from each other – the former involves fourth order equations and is conformally invariant, while the latter shares none of these. For this reason, at the very outset in our paper, we clarified that we were not talking of merging or mapping the two theories entirely into one another (*p.4*) but concentrating only on a particular common prediction.

Similarly, despite differences in the EiBI theory and the MO model, our identification $R_{\text{DM}} = R_{\text{WR}}$ leads to constraints on ρ_0 that are found to be remarkably compatible with the independent NFW or Burkert data fits – that is, the fitted central density values do fall within the stability induced limits. This is the *a posteriori* justification for using the identity $R_{\text{DM}} = R_{\text{WR}}$.

Fit of v_{tg}^2 of Eq.(15) with the observed rotational data [107] reveals that the constant γ ($\equiv N^*\gamma^* + \gamma_0$) is of the order of 10^{-30} cm^{-1} since $N^* \approx 10^{11}$ (roughly, the number of stellar units in a galactic luminous mass). Also, the estimates covering all samples in [44] reveal that the luminous masses lie approximately in the range $M = N^*\beta^* \approx 10^{14} - 10^{16} \text{ cm}$ and from the fitted value of $\gamma^* = 5.42 \times 10^{-41} \text{ cm}^{-1}$, it follows that $N^*\gamma^* \approx 10^{-30} \text{ cm}^{-1}$. Thus at halo distances ($R > 4R_0$), we can ignore the last two terms in (18) by order of magnitudes. In the same manner, we see that $M\gamma \ll 1$ and it may be easily ignored in (13) so that $(1 - 6M\gamma)^{1/2} \simeq 1$. Thus the theoretical metric (13) and the fitted metric (18) coincide at the form

$$B(r) \simeq 1 - \frac{2M}{r} + \gamma r - kr^2 \quad (18)$$

at halo distances $R > 4R_0$. This is also the form of the Weyl solution used in Refs. [48,89]. Rephrasing, we can say that v_{tg}^2 can be arrived at by differentiating the metric (17), which in turn approximates to the Weyl solution (18). That's the relevance of the Weyl solution in the fitting program.

In the asymptotic limit, Eq.(15) gives

$$\frac{v_{\text{tg}}^2}{R} \rightarrow \frac{N^*\beta^*c^2}{R^2} + \frac{N^*\gamma^*c^2}{2} + \frac{\gamma_0c^2}{2} - kc^2R, \quad (19)$$

in which one recognizes the Schwarzschild-like potential $V_{\beta^*} = N^*\beta^*c^2/R$, two linear potential terms, viz., a local $V_{\gamma^*} = N^*\gamma^*c^2R/2$ associated with the matter distribution within a galaxy and a global $V_{\gamma_0} = \gamma_0c^2R/2$ associated with the cosmological background, while the universal de Sitter-like quadratic potential term $V_k = -kc^2R^2$ is induced by inhomogeneities in the cosmic background. Note that the last three potentials are new inputs into the MO model [48] designed to interpret the rotation curve data.

The radial geodesic in the metric (12) is given by

$$\left(\frac{dr}{dt}\right)^2 = B^2(r) - a\frac{B^3(r)}{r^2} - bB^3(r), \quad (20)$$

where a and b are constants of motion. The right hand side of the above equation is the "effective potential" V , and $V''_{\text{MO}} \equiv f(R)$ involves the derivatives of $B(R)$ that, in turn, contains the so called quadratic potential V_k ($= -kc^2R^2$) introduced in Ref.[48]. [The subscript "MO" is used here to distinguish it from the potential V_{EiBI} to be defined in Eq.(22)]. This potential V_k is responsible for providing a finite radius R_{WR} .

The main reason is the *negative sign* in V_k needed for the data fit by MO. Because of this, it is quite evident from the plot of V''_{MO} [Fig.(2)] that the sample ESO 1200211 has a maximally allowed finite halo radius $\sim 39.033 \text{ kpc}$ (see also [100] for similar plots). On the other hand, if V_k has a positive sign (in which case no fit to data) or is altogether removed from

$B(R)$, hence from V''_{MO} , it can be graphically verified that there will be *no* finite stable radius R_{WR} for the halo. This shows the crucial role of V_k . Thus, it is the requirement of fitting to data that indirectly limits the halo size to R_{WR} . As to the physical reason, we see that the repulsive potential V_k balances the remaining attractive potentials at $r = R_{\text{term}}$ [see Eq.(15)] but stability further demands that $R_{\text{WR}} < R_{\text{term}}$, as is evident from Figs.1 & 2. Therefore, we can say that, at $r = R_{\text{WR}}$, attractive potentials prevail over the repulsive potential V_k constraining the gas on the circular orbit, as it should.

The right hand side of Eq.(20) and its first derivative with respect to r , both must vanish at the circular radius $r = R$ giving

$$a = \frac{R^3 B'(R)}{2B^2(R)}, \quad b = \frac{2B(R) - RB'(R)}{2B^2(R)}.$$

The condition for stability is that the second derivative of the “effective potential” V with respect to r must be negative at the circular radius $r = R$. The resultant expression with values of a, b plugged in leads to the generic stability criterion for the MO model:

$$V''_{\text{MO}} = 2B'^2(R) - B(R)B''(R) - 3B(R)B'(R)/R < 0. \quad (21)$$

This inequality graphically predicts a *finite, stable, maximum* halo radius that we call R_{WR} caused solely by the quadratic potential $V_k(R) = -kc^2 R^2$. Interestingly, the predicted R_{WR} lends itself to observational testing in the near future as its value does not often much exceed the R_{last} for many samples.

We shall apply the above algorithm to many samples but for illustration, we display V''_{MO} vs R for the same sample ESO 1200211 in Fig.2. The value of N^* can be found from $N^* = M_{\text{lum}}/\beta^*$, where $M_{\text{lum}} = [(M/L)_{\text{stars}} \times L_{\text{B}} + M_{\text{HI}}] \times 10^{10} M_{\odot}$. All necessary components can be read off from the entries in the *Table IV* in [107]. The value of N^* ($= 5.60 \times 10^7$) together with other constants in (15), when plugged into the inequality (21), immediately graphically yields $R = R_{\text{WR}} = 39.03$ kpc, which is less than R_{term} calculated above.

III. UPPER LIMIT DENSITY FOR STABILITY

To analyze the stability of circular orbits, one needs to analyze the second order derivative of the concerned potential, which we wish to do here. To find the potential V , note that the four velocity $U^\alpha = \frac{dx^\alpha}{d\tau}$ of a test particle of rest mass m_0 moving in the halo (restricting ourselves to $\theta = \pi/2$) follows the equation $g_{\nu\sigma} U^\nu U^\sigma = -m_0^2$ that can be cast into a Newtonian form in the dimensionless radial variable \bar{r} ($= \pi r/R_{\text{DM}}$) as

$$\left(\frac{d\bar{r}}{d\tau}\right)^2 = E^2 + V_{\text{EiBI}}(\bar{r}) \quad (22)$$

which gives, for the metric Eqs.(7)-(10) of Sec.II(a), the EiBI potential

$$V_{\text{EiBI}}(\bar{r}) = \left[E^2 \left\{ \frac{1}{AB} - 1 \right\} - \frac{L^2}{AC\bar{r}^2} - \frac{1}{A} \right] \quad (23)$$

$$E = \frac{U_0}{m_0}, L = \frac{U_3}{m_0}, \quad (24)$$

where the constants E and L , respectively, are the conserved relativistic energy and angular momentum per unit mass of the test particle. Circular orbits at any arbitrary radius are defined by $\bar{r} = \bar{R} = \text{constant}$, so that $\frac{d\bar{r}}{d\tau} |_{\bar{r}=\bar{R}} = 0$ and, additionally, $\frac{dV}{d\bar{r}} |_{\bar{r}=\bar{R}} = 0$. From these two conditions follow the conserved quantities as under:

$$L^2 = \frac{X}{Z} \quad (25)$$

and using it in $V_{\text{EiBI}}(\bar{R}) = -E^2$, we get

$$E^2 = \frac{Y}{Z}, \quad (26)$$

where

$$X \equiv -\kappa^2 \bar{R}^3 v_\infty^2 (\bar{R} - \bar{\rho}_0 \sin \bar{R})^2 \quad (27)$$

$$Y \equiv \left(\kappa \bar{R}^2 + 2r_0^2 r_{\text{opt}}^2 \right) \left(r_0^2 + \frac{\kappa \bar{R}^2}{2r_{\text{opt}}^2} \right)^{v_\infty^2} (\bar{\rho}_0 \bar{R} \cos \bar{R} + \bar{\rho}_0 \sin \bar{R} - 2\bar{R}) \quad (28)$$

$$Z \equiv \left\{ \kappa \bar{R}^2 (1 - 2v_\infty^2) + 2r_0^2 r_{\text{opt}}^2 \right\} \bar{\rho}_0 \sin \bar{R} + \left(\kappa \bar{R}^2 + 2r_0^2 r_{\text{opt}}^2 \right) \bar{\rho}_0 \bar{R} \cos \bar{R} - 4\bar{R} r_0^2 r_{\text{opt}}^2 - 2\kappa \bar{R}^3 (1 - v_\infty^2). \quad (29)$$

Putting the expressions for L^2 and E^2 in Eq.(23), we find the complete expression for V_{EiBI} . The orbits will be stable if $V''_{\text{EiBI}} \equiv \frac{d^2 V}{d\bar{r}^2} |_{\bar{r}=\bar{R}} < 0$ and unstable if $V''_{\text{EiBI}} > 0$. The expression for V''_{EiBI} is

$$\begin{aligned}
& V''_{\text{EiBI}}(\bar{R}; \kappa, \bar{\rho}_0, r_0, r_{\text{opt}}, v_\infty) \\
= & \left[\frac{2v_\infty^2 (\bar{R} + \bar{\rho}_0 \bar{R} \cos \bar{R} - \bar{\rho}_0 \sin \bar{R})}{\bar{R}^2 (\kappa \bar{R}^2 + 2r_0^2 r_{\text{opt}}^2)} Z \right] \times \\
& \left[32\bar{R}^2 r_0^2 r_{\text{opt}}^2 + 8\kappa \bar{R}^4 (1 - v_\infty^2) + 6\bar{\rho}_0^2 r_0^2 r_{\text{opt}}^2 (1 + \bar{R}^2) \right. \\
& + \kappa \bar{\rho}_0^2 \bar{R}^2 (1 - 2v_\infty^2 + 3\bar{R}^2) \\
& - 2\bar{R}^2 \left\{ 14r_0^2 r_{\text{opt}}^2 + \kappa \bar{R}^2 (5 - 2v_\infty^2) \right\} \bar{\rho}_0 \cos \bar{R} \\
& + \left\{ 2(\bar{R}^2 - 3) r_0^2 r_{\text{opt}}^2 - \kappa \bar{R}^2 (1 - 2v_\infty^2 - \bar{R}^2) \right\} \bar{\rho}_0^2 \cos(2\bar{R}) \\
& - \left\{ 36r_0^2 r_{\text{opt}}^2 + 4\bar{R}^2 r_0^2 r_{\text{opt}}^2 + 6\kappa \bar{R}^2 + 2\kappa \bar{R}^4 - 12\kappa \bar{R}^2 v_\infty^2 \right\} \bar{\rho}_0 \bar{R} \sin \bar{R} \\
& \left. + \left\{ 6r_0^2 r_{\text{opt}}^2 + \kappa \bar{R}^2 - 2\kappa \bar{R}^2 v_\infty^2 \right\} \bar{\rho}_0^2 \bar{R} \sin(2\bar{R}) \right]. \tag{30}
\end{aligned}$$

From the above expression, it is absurd to straightforwardly draw any conclusion about stability or otherwise of the circular orbits. Clearly, much will depend on the parameter ranges chosen on the basis of physical considerations. While other parameters can be reasonably assigned, the as yet unknown parameters are the dark matter radius κ ($= 2R_{\text{DM}}^2/\pi^2$) and the dimensionless central density $\bar{\rho}_0$ ($= 8\rho_0 R_{\text{DM}}^2/\pi$), again depending only on κ . In the first order approximation, the density distribution in the dark matter has been assumed in [95,96] to be low such that $8\pi G\kappa\rho^{(0)}/c^4 \ll 1$, but the central density ρ_0 could still be large since $|\sin(x)/x| \leq 1$ [see Eq.(3)]. The question therefore is how large or small could it be, or turning it around, could there be any upper limit on ρ_0 imposed by the stability criterion?

The answer is in the affirmative and can be found graphically. We find that V'' is indeed very sensitive to changes in ρ_0 leading to different upper limits ρ_0^{upper} for different galactic samples such that stable circular orbits are possible only when $\rho_0 \leq \rho_0^{\text{upper}}$. The reason is that R_{DM} changes from sample to sample, as it should, and thereby leads to different (though not too different) values for κ and ρ_0^{upper} . Let us again consider the previous sample ESO 1200211, a low surface brightness galaxy with a halo/dark matter radius $R_{\text{WR}} \equiv R_{\text{DM}} = 39.03$ kpc that corresponds to $\kappa = 308.74$ kpc². With κ thus fixed, we fix other parameters respecting the Newtonian approximation⁹, e.g., $r_0 = 0.61$, $v_\infty^2 = 0.000001$, $r_{\text{opt}} = 8$ kpc, with the dimensionless

⁹The range of r and r_{opt} is chosen so as to ensure the Newtonian approximation $r/r_{\text{opt}} \gg r_0$, while the approximate value of v_∞^2 is an observed fact. The formula for r_0 for spiral galaxies is $r_0 = 1.5 \times (L_{\text{B}}/10^{10.4} L_\odot)^{1/5}$, which evaluates to $r_0 = 0.61$ for the sample ESO 1200211, where $r_{\text{opt}} \simeq 4R_0$, $L_{\text{B}} = 0.028 \times 10^{10} L_\odot$, $R_0 = 2$ kpc. Data taken from [107].

radius \bar{R} ($= \pi R/R_{\text{DM}}$) chosen in the range $\bar{R} \in [0.5\pi, \pi]$ corresponding to coordinate radii $R \in [19.52 \text{ kpc}, 39.03 \text{ kpc}]$, the dimensionless density parameter chosen in the range $\bar{\rho}_0 \in [0.25\pi, 0.8\pi]$ and plot V''_{EiBI} vs \bar{R} using the expression (30).

Graphical analysis shows that, while V''_{EiBI} is not much sensitive to the variation of the other parameters within the Newtonian approximation, it is *greatly* sensitive to the variation of the remaining parameter ρ_0 . Figs. 3 and 4 respectively show that, for values of $\bar{\rho}_0 > 0.94$, there is instability in the entire or partial range of the halo radii \bar{R} , while Fig. 5 tells us that there is an upper limit occurring at $\bar{\rho}_0^{\text{upper}} = 0.94 = \lambda^{\text{upper}}\pi$, where $\lambda^{\text{upper}} = 0.299$, such that for $\bar{\rho}_0 \leq \bar{\rho}_0^{\text{upper}}$, all circular orbits in the entire chosen radial range for \bar{R} are stable. It can be verified that this value of λ^{upper} surprisingly remains the *same* for values for κ across the entire range of 111 samples (some tabulated here), so ρ_0^{upper} is quite a reliable limit.

Rewriting in terms of ρ_0 , we have

$$\rho_0^{\text{upper}} = \frac{\bar{\rho}_0^{\text{upper}}\pi}{8R_{\text{DM}}^2} = \frac{\lambda^{\text{upper}}}{4\kappa}. \quad (31)$$

This by itself is an interesting prediction of EiBI theory. However, if we want to quantify ρ_0^{upper} for a given galaxy, we need to use the value of R_{DM} but since concrete observed values are yet unavailable, we choose to use the input $R_{\text{DM}} = R_{\text{WR}}$. It turns out that this choice, though not mandatory, works well giving definitive values for ρ_0^{upper} for all samples. Plugging in the values of λ^{upper} and κ , we find that the constraint $\bar{\rho}_0 \leq \bar{\rho}_0^{\text{upper}}$ immediately translates into a generic constraint such that for

$$\rho_0 \leq \rho_0^{\text{upper}}, \quad (32)$$

all circular orbits in the chosen range for R are stable. Thus, using the value of κ as above in Eq.(31), the sample ESO 1200211 quantitatively yields $\rho_0^{\text{upper}} = 5.04 \times 10^{12} M_{\odot}\text{kpc}^{-3}$. In general, as long as ρ_0 of any galaxy obeys the stability induced constraint (32), the circular material orbits in the halo region will be stable up to a *maximum* radius $R = R_{\text{WR}}$.

IV. CENTRAL AND MEAN DARK MATTER DENSITY

So far, the algorithm has been as follows: Take any galactic sample, find R_{WR} for that sample using the method of Sec.II(b). Then, from the identity $R_{\text{DM}} = R_{\text{WR}}$, find R_{DM} (hence κ) and using Eq.(31), find ρ_0^{upper} . However, we still do not know the values of ρ_0 for all the samples observed to date and cannot ascertain whether or not they satisfy the stability induced constraint $\rho_0 \leq \rho_0^{\text{upper}}$. On the other hand, some notable dark matter simulations and profiles for several samples show values for ρ_0 that *do* respect this constraint (Table II). This success then prompts us to ask if there is any lower limit on ρ_0 such that $\rho_0^{\text{lower}} \leq \rho_0 \leq \rho_0^{\text{upper}}$ holds.

Fortunately, there is a way to find the values of ρ_0^{lower} , once we are able to estimate the total mass of dark matter M_{DM} using the observed mass-to-light ratios. Fitted data are available for the luminous mass-to-light ratios ($M_{\text{lum}}/L_{\text{B}}$) in solar units Υ_{\odot} ($\equiv \frac{M_{\odot}}{L_{\odot}}$):

$$\frac{M_{\text{lum}}}{L_{\text{B}}} = \gamma \Upsilon_{\odot}.$$

The luminous mass (M_{lum}) of a galaxy is contributed mostly by stars and gases excluding dark matter. The stellar mass-to-light ratios γ for 111 samples in [107] are seen to lie between 0.2 and 8 (with just a couple of exceptions), which is consistent with the upper bound of $10\Upsilon_{\odot}$ suggested by the population synthesis models [109]. On the other hand, there is no detectable dark matter associated with the galactic disk, most of the dark matter is distributed in the halo [110-114]. So we can write

$$M_{\text{tot}} = M_{\text{lum}} + M_{\text{DM}}, \quad (33)$$

then

$$\frac{M_{\text{tot}}}{L_{\text{B}}} = \beta \Upsilon_{\odot}$$

where β must be larger than γ , if there is dark matter (observed mass-to-light ratios are still uncertain). We can thus write, following Edery & Paranjape [89]:

$$\frac{M_{\text{lum}}}{M_{\text{tot}}} = \frac{1}{\alpha}, \quad (34)$$

which gives $\beta = \alpha\gamma$ and α should be so chosen as to make $\beta > \gamma$. In general, one takes $\alpha > 1$ such that $M_{\text{tot}} > M_{\text{lum}}$ thereby accommodating the presence of dark matter.

Assuming that the halos must be substantially larger than the last measured point R_{last} , the dark to luminous mass within R_{last} then gives an upper limit through $f_b < \frac{M_{\text{lum}}}{M_{\text{tot}}}$ and therefore $f_b < \left(1 + \frac{M_{\text{DM}}}{M_{\text{lum}}}\right)^{-1}$. For some galaxies, $f_b < 0.08$, as reported in de Blok and McGaugh [115]. Thus, using (34), we have $f_b < \frac{1}{\alpha}$ and $f_b < 0.08$. Certainly, these inequalities do not constrain α in any way. One of the infinity of options to ensure that both hold simultaneously is to assume that $\frac{1}{\alpha} = 0.08 \Rightarrow \alpha = 12.5$. While α can be varied at will unless it is definitively fixed by independent concrete observed data, we shall for the moment choose the value $\alpha = 12.5$ only to have an idea of the order of magnitudes of the estimated densities, but we shall change α later. The current choice would imply $\beta \in [2.5, 100]$ corresponding to $\gamma \in [0.2, 8]$. The values of $\beta \sim 100$ is enough to account for the large dark matter content of LSB galaxies (i.e., large mass-to-light ratios $\frac{M_{\text{tot}}}{L_{\text{B}}}$) such as DDO154. Currently favored Burkert density profile can provide an excellent mass model for the dark halos around disk systems up to 100 times

more massive than small dwarf galaxies for which the profile was initially intended [116,117].

The ratio $M_{\text{lum}}/M_{\text{tot}}$ then gives the connection between M_{DM} of EiBI theory and the luminous mass M_{lum} of galaxies via Eq.(33):

$$M_{\text{DM}} = (\alpha - 1)M_{\text{lum}}. \quad (35)$$

Using $R_{\text{WR}} \equiv R_{\text{DM}}$, Eq.(6) can be rewritten as

$$\rho_0^{\text{lower}} = \frac{\pi(\alpha - 1)M_{\text{lum}}}{4R_{\text{WR}}^3}, \quad \langle \rho \rangle^{\text{lower}} = \frac{3\rho_0^{\text{lower}}}{\pi^2}. \quad (36)$$

The superscript "lower" indicates that it is the lower limit of the dark matter central density ρ_0 because R_{WR} is the maximum allowed halo radius (see Fig.2), where $V'' < 0$ gives stable radii $R \leq R_{\text{WR}}$. Evidently, ρ_0^{lower} is proportional to the as yet unknown parameter α . We are free to raise the value of α arbitrarily, but then the consequent larger values of β would lead to too large an amount of dark matter comparable to that existing in galactic clusters.¹⁰

To illustrate the order of magnitudes involved for ρ_0^{lower} , hence for $\langle \rho \rangle^{\text{lower}}$, we again consider the low mass LSB sample ESO 1200211 for which $M_{\text{lum}} = 5.60 \times 10^7 M_{\odot}$, $\gamma = 0.2$ and our method in Sec.II(b) yields $R_{\text{WR}} = 39.03$ kpc, $\kappa = 308.74$ kpc², $R_{\text{term}} = 52.04$ kpc. Using Eqs.(36), and allowing for a fairly large amount of dark matter over luminous matter corresponding to $\alpha = 12.5$, we find $\rho_0^{\text{lower}} = 8.49 \times 10^4 M_{\odot}\text{kpc}^{-3}$ and $\langle \rho \rangle^{\text{lower}} = 2.58 \times 10^4 M_{\odot}\text{kpc}^{-3}$. To compare these values of density, we consider several dark matter density profiles: (i) the Bose-Einstein [108] condensate (ρ_0^{BEC}), (ii) Pseudo-Isothermal [120] profile (ρ_0^{PI}), (iii) the NFW [121,122] profile (ρ_i^{NFW}), (iv) Burkert [116] profile (ρ^{BP}), (see Sec.V below for the exact forms). They yield values as follows: (i) $\rho_0^{\text{BEC}} = 1.38 \times 10^7 M_{\odot}\text{kpc}^{-3}$, (ii) $\rho_0^{\text{PI}} = 4.64 \times 10^7 M_{\odot}\text{kpc}^{-3}$ and (iii) $\rho_0^{\text{NFW}} = 2.45 \times 10^6 M_{\odot}\text{kpc}^{-3}$ for ESO 1200211 (see the entries in *Table I* of [108]). In Sec.III, we already found for the present sample the value $\rho_0^{\text{upper}} = 5.04 \times 10^{12} M_{\odot}\text{kpc}^{-3}$. We hence see that the central densities from different profiles fall within the stability induced limits, that is, $\rho_0^{\text{lower}} < \rho_0^{\text{BEC, PI or NFW}} < \rho_0^{\text{upper}}$ holds.¹¹ If we take $\alpha < 12.5$, which should also be quite acceptable for many

¹⁰At much larger scales of galactic clusters, the value of β could be ≥ 120 [118,119] so that $\frac{M_{\text{tot}}}{L_{\text{B}}} \geq 120$ in solar units. We are not contemplating galactic clusters here.

¹¹Once again, a question of compatibility might be phrased as follows: The EiBI density profile has $\rho(R_{\text{DM}}) = 0$ and remains zero beyond $r > R_{\text{DM}}$, while, in contrast, the NFW and Burkert profiles have $\rho(r \rightarrow \infty) = 0$. Since the asymptotic behavior of latter density distributions are different from that of EiBI, determining whether the data obtained by fitting to NFW or Burkert profiles fall within the stability induced limits from EiBI theory calls into question the issue of compatibility of the EiBI with those profiles.

We wish to clarify that it is the central density ρ_0 , a parameter distinctly appearing in

samples, the values of ρ_0^{lower} will only be further lowered and of course the interval will be well supported.

If we increase α to an (unlikely) mammoth value, say $\alpha = 300$ so that $M_{\text{tot}} = 300M_{\text{lum}}$ implying $\beta = 60$ so that $\frac{M_{\text{tot}}}{L_{\text{B}}} = 60Y_{\odot}$ in the considered sample, then $\rho_0^{\text{lower}} \sim 2.20 \times 10^6 M_{\odot}\text{kpc}^{-3}$, and we notice that the proposed limits are still not violated! If we exclude NFW profile, then the values α can be increased even further. This testifies to the validity of Eq.(36) as well as the limits.

V. Milky Way

As for our Milky Way galaxy, the latest reported estimates are the following: Using the gas terminal velocity curve, Sgr A* proper motion, an oblate bulge + Miyamoto-Nagai disc and NFW halo, Kafle *et al.* [123] estimated the luminous (disc + bulge) mass to be $M_{\text{lum}} \sim 1.04 \times 10^{11} M_{\odot}$, so that $N^* = 1.04 \times 10^{11}$ and the virial mass inclusive of dark matter $M_{\text{vir}} = M_{\text{tot}} \sim 0.80 \times 10^{12} M_{\odot}$ so that $\alpha = M_{\text{tot}}/M_{\text{lum}} = 7.68$. (We have not considered the data/fit uncertainties). For alternative but not too different values of M_{tot} , see [124-131].¹² Using the scale length $R_0 = 4.9$ kpc [123] and the above N^* in the inequality (21), we find that $R_{\text{WR}} = R_{\text{DM}} = 111.90$ kpc. With this value of R_{WR} , Eq. (31) then yields a value $\rho_{0, \text{MW}}^{\text{upper}} = 6.14 \times 10^{11}$

all density distributions, that is under present investigation. No matter what the profile is, the target is always the same: to find information about ρ_0 for any given galactic sample. We know that NFW profile is cuspy ($\rho^{\text{NFW}} \propto r^{-1}$), while others such as that of Burkert are cored ($\rho^{\text{BP}} \propto r^0$). Despite this radical difference in behavior *at the origin*, both profiles are quite well accepted though *per se* they are different. One could rephrase this difference as incompatibility. The main thing however is that the fitted values of central density from the two profiles should approximately be the same, at least by order of magnitude, which actually is the case [108,132]. (A brief account of comparisons as to which profile fits the data better is given at the very last paragraph of our paper). In the same vein, despite differences in the *asymptotic* behavior of EiBI profile and other density profiles, the information about the common parameter ρ_0 should approximately be the same. It would be fair to say that the derived bound for the central density ρ_0 is indeed in agreement with the astrophysical data but that it is yet to be determined if the EiBI density profile is compatible with future N-body simulation featuring higher accuracy allowing for testing the outskirts of dark matter halos.

Also, it is very unlikely that the attractive dark matter is spread all the way to infinity, where repulsive dark energy takes over. The finite extent of dark matter is supported by the observed rapid decline of velocity dispersion after a certain radius [143]. It could indeed be interesting to take this fact as an empirical input for R_{DM} only if we knew the exact radius at which the decline ended. Pending this knowledge, we used theoretical inputs R_{WR} for R_{DM} , which yielded the interval for ρ_0 confirmed by data fits so far.

¹²In [124], it is reported that $M_{\text{tot}} = (1.4 \pm 03) \times 10^{12} M_{\odot}$ from tidal effects on globular clusters and $M_{\text{tot}} = (1.4 \pm 08) \times 10^{12} M_{\odot}$ from globular cluster radial velocities. The remarkable similarity between two completely independent determinations of mass may be taken as a strong empirical signature for the existence of dark matter around the Milky Way. In [125], the reported estimate is $M_{\text{tot}} = (1.0 - 1.5) \times 10^{12} M_{\odot}$, again not too different.

$M_{\odot}\text{kpc}^{-3}$ characteristic of the Milky way, which does not exceed the maximum density ($\sim 10^{12}M_{\odot}\text{kpc}^{-3}$) proposed in this paper.

The density profiles considered here are of the forms:

$$\rho^{BP}(r) = \frac{\rho_0^{BP} r_0^3}{(r+r_0)(r^2+r_0^2)} = \rho_0^{BP} \left(1 - \frac{r}{r_0} + \frac{r^4}{r_0^4} + \dots\right) \quad [116](37)$$

$$\rho^{NFW}(r) = \frac{\rho_0^{NFW}}{(r/r_S)[1+(r/r_S)^2]} = \rho_0^{NFW} \left(\frac{r_S}{r} - \frac{r}{r_S} + \frac{r^3}{r_S^3} + \dots\right) \quad [121,122] \quad (38)$$

$$\rho^{PI}(r) = \frac{\rho_0^{PI}}{1+(r/r_c)^2} = \rho_0^{PI} \left(1 - \frac{r^2}{r_c^2} + \frac{r^4}{r_c^4} + \dots\right) \quad [120] \quad (39)$$

$$\rho^{BEC}(r) = \rho_0^{BEC} \left[\frac{\sin(\xi r)}{\xi r}\right] = \rho_0^{BEC} \left(1 - \frac{\xi^2 r^2}{6} + \frac{\xi^4 r^4}{120} + \dots\right) \quad [108] \quad (40)$$

where ρ_0 is the galactocentric density, ρ_0^{NFW} is related to the density of the universe at the moment the halo collapsed and r_0 , r_S , r_c are core, scale, characteristic radii respectively, while $\xi = \sqrt{Gm^3/\hbar^2 a}$ in which m is the mass of the dark matter particle and a is the scattering length [108]. The fitted latest data on Milky Way dark matter central density are $\rho_0^{BP} = 4.13 \times 10^7 M_{\odot}\text{kpc}^{-3}$ (Burkert profile) and $\rho_0^{NFW} = 1.40 \times 10^7 M_{\odot}\text{kpc}^{-3}$ (NFW profile) [132]. In both cases, we see that these fitted values are four orders of magnitude *less* than $\rho_{0,MW}^{\text{upper}}$, as desired. From Eq.(36), for $\alpha \sim 7.68$, we get $\rho_{0,MW}^{\text{lower}} \sim 2.09 \times 10^3 M_{\odot}\text{kpc}^{-3}$ and $\langle \rho \rangle_{0,MW}^{\text{lower}} \sim 6.37 \times 10^2 M_{\odot}\text{kpc}^{-3}$. Once again, we see that the densities satisfy $\rho_0^{\text{lower}} < \rho_0^{BP, NFW} < \rho_0^{\text{upper}}$. A larger value of α does not disallow the inequalities at either end.

Apart from the galactocentric density ρ_0 , the local (at $R_{\odot} = 8.5$ kpc) dark matter density ρ_{\odot} provides a strong basis for the experimental endeavors for indirect detection of the dark matter. Though there is broad consensus, different groups have come up with somewhat different conclusions regarding the local density of dark matter. For example, Kuijken and Gilmore [111-114] find a volume density near Earth $\rho_{\oplus} \simeq 0.01 \text{ GeV}/\text{cm}^3 = 2.64 \times 10^5 M_{\odot}\text{kpc}^{-3}$. Other reported values are the following. Bahcall *et al.* [133] find a best-fit value of $\rho_{\odot} = 0.34 \text{ GeV}/\text{cm}^3 = 8.96 \times 10^6 M_{\odot}\text{kpc}^{-3}$, Caldwell and Ostriker [134] find $\rho_{\odot} = 0.23 \text{ GeV}/\text{cm}^3 = 6.07 \times 10^6 M_{\odot}\text{kpc}^{-3}$, while Turner [135] calculates $\rho_{\odot} = 0.3 - 0.6 \text{ GeV}/\text{cm}^3 = 7.92 \times 10^6 - 1.58 \times 10^7 M_{\odot}\text{kpc}^{-3}$. For a more comprehensive discussion on the distribution of dark matter, see [136]. The local dark matter energy density, consistent with standard estimates, is $\rho_{\odot} = (0.3 \pm 0.1) \text{ GeV}/\text{cm}^3 = 7.92 \times 10^6 M_{\odot}\text{kpc}^{-3}$ [137]. Bergstrom, Ullio and Buckley [69] find local dark matter densities acceptable in a somewhat broad range $0.2 - 0.8 \text{ GeV}/\text{cm}^3$. The fitting with Burkert profile yields $\rho_{\odot}^{BP} = 0.487 \text{ GeV}/\text{cm}^3 = 1.28 \times 10^7 M_{\odot}\text{kpc}^{-3}$ and fitting with NFW profile yields $\rho_{\odot}^{NFW} = 0.471 \text{ GeV}/\text{cm}^3 = 1.24 \times 10^7 M_{\odot}\text{kpc}^{-3}$ [132]. About sys-

tematic uncertainties in the determination of local density of dark matter, see [139]. Overall, one could fairly say that $\rho_{\odot} \propto 10^6 - 10^7 M_{\odot} \text{kpc}^{-3}$.

We use the above local values as a constraint to estimate the central density ρ_0^{BEC} given in Eq.(40) that approaches a constant value ρ_0^{BEC} as $r \rightarrow 0$ (so does the EiBI profile $\rho^{(0)}(r)$ in Eq.(3) as the two are essentially of the same form). This behavior is consistent with the currently favored core behavior at the galactic center, as opposed to the NFW cusp. To estimate the values of ρ_0^{BEC} for the Milky Way, we constrain the BEC profile such that it coincides with the local value $\rho_{\odot}^{BP} = 1.28 \times 10^7 M_{\odot} \text{kpc}^{-3}$ at $R_{\odot} = 8.5 \text{ kpc}$ (boundary condition). This then yields a central density $\rho_0^{BEC} = 1.29 \times 10^7 M_{\odot} \text{kpc}^{-3}$. This is quite an acceptable central density value for the Milky Way. (We could as well use the same boundary condition using ρ_{\odot}^{NFW} , but it does not lead to a much different value for ρ_0^{BEC}). Having determined the value of ρ_0^{BEC} , we compare it with the corresponding values from NFW and Burkert profiles using data from [132] and observe the following: (i) ρ_0^{BEC} is quite comparable with ρ_0^{BP} and ρ_0^{NFW} , (ii) the NFW cusp and the PI, Burkert core behavior are evident from Fig. 6. (iii) Identifying the BEC constant $\xi \equiv \frac{\pi}{R_{DM}}$, we see that the ρ^{BEC} profile shows a *much slower* monotonic decline from its central value ρ_0^{BEC} , coasting along almost flat all the way up to a finite R_{DM} ($= 111.90 \text{ kpc}$, in the present case), where it vanishes, (iv) adopted values from the Burkert profile has allowed us to predict ρ_0^{BEC} , which is seen also to be included in the limiting interval, $\rho_0^{\text{lower}} < \rho_0^{BEC, BP, NFW} < \rho_0^{\text{upper}}$ for the Milky Way.

Returning to the profiles (39) and (40), it is remarkable that the PI and BEC profiles have the same behavior up to second order in r provided we identify $r_c = \frac{\sqrt{6}}{\xi}$ but they begin to differ in the higher order coefficients thereafter. Also, it is known that the large majority of the high-resolution rotation curves prefer the PI core-dominated halo model, which provide a better description of the data than the cuspy ($\rho^{NFW} \propto r^{-1}$) NFW profile [140]. In this sense, the EiBI model could be a competing candidate to PI model. It would be our future task to investigate where these two models agree and where they disagree.

VI. CONCLUSIONS

The present paper, based on a pivotal input from Weyl gravity, viz., $R_{DM} = R_{WR}$ (motivated by [89]), offers a new alternative *analytical* window, different from the standard data-fit approaches, to look at the physical galactic parameters. While the latter approaches are technically more elaborate, and the current EiBI analytic approach is not, the value of the paper lies in the fact that it can still make quantitative predictions about the limits on central dark matter density ρ_0 . Many samples for which the values of ρ_0 are available are shown to satisfy the inequality $\rho_0 \leq \rho_0^{\text{upper}} \propto R_{WR}^{-2} \sim 10^{12} M_{\odot} \text{kpc}^{-3}$. Only some samples are tabulated here. Table I shows the

halo/dark matter radius, the velocity terminating radius R_{term} and the corresponding coupling parameter κ .

Going a step further, we also calculated $\rho_0^{\text{lower}} \propto (\alpha - 1)M_{\text{lum}}R_{\text{WR}}^{-3}$ that depends on a certain parameter α equal to the ratio of luminous to total (dark matter included) mass of a galaxy. Definitive estimates of such ratios are yet unavailable. Nevertheless, it is shown that (Table II), for reasonably wider values of α (≥ 12.5) accounting for huge quantities of dark matter in individual samples, profile dependent values of ρ_0 still fall inside the EiBI predicted interval $\rho_0^{\text{lower}} \leq \rho_0 \leq \rho_0^{\text{upper}}$. These limits cover a large class of galaxies and indicate an interesting facet of the EiBI theory. We especially point out that the maximal value $\rho_0^{\text{upper}} \propto R_{\text{WR}}^{-2} \sim 10^{12} M_{\odot}\text{kpc}^{-3}$ is purely a stability induced constraint on all galaxies with dark matter, while $(\alpha - 1)M_{\text{lum}}R_{\text{WR}}^{-3} \propto \rho_0^{\text{lower}} \leq \rho_0$ is not, due to uncertainties in α . Thus, we would particularly advocate a practical verification of ρ_0^{upper} ($\propto 1/\kappa$) rather than ρ_0^{lower} . If verified, it would also mean that we have a clearcut theoretical algorithm, applicable to all galactic samples, that provides a definitive, falsifiable information on the radius R_{DM} of dark matter/halo – something that seems rather scarce in the astrophysical literature.

A special merit of the foregoing analyses is that the only information needed to calculate the above limits are those of the fitted luminous M_{lum} values and the measured total mass M_{tot} . Note that a small change in M_{lum} would lead to a large change in R_{WR} . For instance, there is an argument [117,141] for an upper mass limit indicated by the sudden decline of the visible baryonic mass function of disk galaxies at $M_{\text{disc}}^{\text{max}} = 2 \times 10^{11} M_{\odot}$. Tentatively assuming that the luminous part of the Milky Way mass M_{lum} is $2 \times 10^{11} M_{\odot}$ instead of $1.04 \times 10^{11} M_{\odot}$, then the resultant R_{WR} would jump to 177.94 kpc from 111.90 kpc. Similarly, R_{term} would jump to 238 kpc from 150.17 kpc. Thus, for reliable values of R_{WR} , the luminous mass data M_{lum} should be as accurate as possible.

We have verified that quantitative upper limit $\rho_0^{\text{upper}} \sim 10^{12} M_{\odot}\text{kpc}^{-3}$ is respected by all the samples collected in [107], some of which are given in Table II. The reason for such consistency is not accidental – it stemmed from the fact that the Weyl radius R_{WR} has a solid foundation: The rotation curve is a *prediction* of Weyl gravity MO solution containing constants (γ_0, γ^*, k) that are universally applicable to all the galaxies¹³, LSB or HSB, and that the R_{WR} is a straightforward result from $V'' < 0$. In fact, the reported data on R_{last} for individual samples have so far been found to obey

¹³The claim is grounded to the fact that a single set of universal constants (γ_0, γ^*, k) and the (M/L) ratio of individual samples, all *a priori* known, are enough to nicely predict all the rotation data – no adjustable free parameters are needed. In contradistinction, NFW, Burkert, PI or other profiles only give the generic shapes of halos, and leave the values for ρ_0 and r_0 as free parameters to be finely tuned to data galaxy by galaxy. This procedure then quickly generates large numbers of such values as more and more galactic rotation curves are considered (For details of such "fine tuning", see [35], pp. 32,33).

$R_{\text{last}} < R_{\text{WR}}$. So we conjectured that this radius R_{WR} just might be *the* dark matter radius R_{DM} specific to individual galaxies.

As we saw, the constraint $\rho_0 \leq \rho_0^{\text{upper}} \sim 10^{12} M_{\odot} \text{kpc}^{-3}$ is a necessary condition for stability of circular orbits. Whether it is also a sufficient condition, that is, whether there are no stable orbits in the halo if this constraint is violated, is a matter of independent practical verification. If sufficiency turns out to be true, then we might expect to observe galaxies with no information on dark matter due to lack of stable circular orbits. It may be noted that our $\rho_0^{\text{upper}} \sim 6.14 \times 10^{11} M_{\odot} \text{kpc}^{-3}$ for Milky Way is remarkably consistent with the *local upper limit* on the dark matter density in the solar system, $\rho_{\odot}^{\text{upper}} \sim 2.94 \times 10^{12} M_{\odot} \text{kpc}^{-3}$, found by completely different methods and ideas [142].

There are limitations with almost all well known density profiles in the sense that they fit the data so well in one sector, but fail in the other. For instance, it has been argued [143] that the NFW profile does not always follow from the gas rotation curves of large samples. For a constant velocity anisotropy, the PI profile is ruled out, while a truncated flat (TF) model [144] and NFW model are consistent with the data. Incidentally, it might be noted that the TF model expands up to r^2 like both in the PI and BEC profiles, and further, like the MO model, TF is described solely by two parameters, mass and the scale length. Nesti and Salucci [132] argue that NFW and/or PI halos are not supported by present day observations in external galaxies due to recent improvement of simulation techniques. URC profile for velocity distribution seems to fit the data incredibly well up to ~ 30 kpc [97]. The present model based on EiBI Eq.(3), which is akin to the quantum BEC model, is probably no better or worse than the others. Nevertheless, the foregoing study hopefully provides some new definitive information in an analytic way using a metric solution (7) of EiBI theory.

Table I. Lower bound on average density [eq. (36)].

Galaxy $\alpha = 12.5$	R_{WR} (kpc)	R_{term} (kpc)	κ (kpc) ²	$\langle \rho \rangle^{\text{lower}}$ ($M_{\odot} \text{kpc}^{-3}$)	γ	$\beta = \alpha\gamma$
ESO1870510	39.66	52.96	318.83	2.45×10^4	1.62	20.25
ESO3020120	44.77	60.15	406.11	1.71×10^4	1.07	13.37
ESO3050090	39.45	52.65	315.37	2.49×10^4	0.32	04.00
ESO4880490	42.25	56.62	361.70	2.03×10^4	3.07	38.37
U04115	39.02	52.03	308.53	2.58×10^4	0.97	12.12
U11557	41.75	55.91	353.21	2.11×10^4	0.20	02.50
U11748	106.18	142.57	2284.84	1.28×10^3	0.40	05.00
U11819	72.80	98.08	1073.95	3.97×10^3	2.24	28.00
U11583	39.08	52.11	309.47	2.57×10^4	0.70	08.75
F568-3	50.10	67.53	508.76	1.22×10^4	4.2	52.50
F583-1	41.50	55.57	349.11	2.14×10^4	1.6	20.00

Table II. Central densities of dark matter and upper bounds [eq. (31)]. All densities are in units of $M_{\odot}\text{kpc}^{-3}$, $\alpha = 12.5$

Galaxy	ρ_0^{lower}	ρ_0^{BEC}	ρ_0^{PI}	ρ_0^{NFW}	ρ_0^{upper}
ESO 1870510	8.08×10^4	3.29×10^7	5.48×10^7	7.61×10^5	4.88×10^{12}
ESO 3020120	5.63×10^4	2.29×10^7	5.98×10^7	2.65×10^6	3.83×10^{12}
ESO 3050090	8.22×10^4	2.17×10^7	2.76×10^7	3.28×10^7	4.93×10^{12}
ESO 4880490	6.69×10^4	5.49×10^7	1.03×10^8	1.42×10^6	4.30×10^{12}
U04115	8.49×10^4	1.43×10^8	1.51×10^8	1.39×10^5	5.04×10^{12}
U11557	6.94×10^4	4.69×10^9	1.57×10^7	1.08×10^4	4.41×10^{12}
U11748	4.21×10^3	4.20×10^8	1.67×10^9	2.04×10^8	6.81×10^{11}
U11819	1.30×10^3	5.39×10^7	8.69×10^7	1.19×10^6	1.45×10^{12}
U11583	8.45×10^4	9.53×10^7	1.19×10^8	1.36×10^5	5.03×10^{12}
F568-3	4.01×10^4	2.48×10^7	3.61×10^7	3.78×10^5	3.06×10^{12}
F583-1	7.05×10^4	1.90×10^7	3.17×10^7	3.45×10^5	4.46×10^{12}

Figure captions

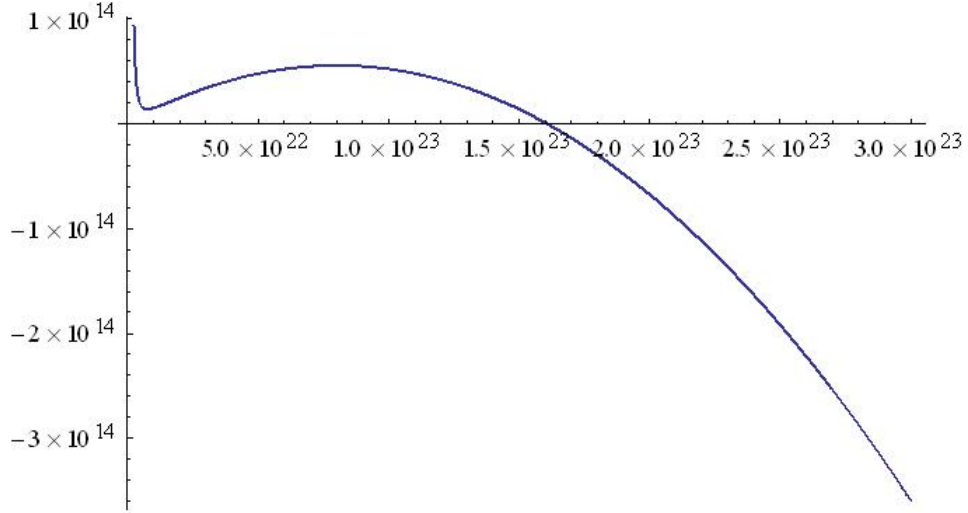


Figure 1: Plot of v_{tg}^2 vs R (cm) using Eq.(15) for ESO 1200211. The luminous mass is $M_{lum} = 5.6 \times 10^7 M_{\odot}$ so that $N^* = 5.6 \times 10^7$. The other constants are in (16) and $R_0 = 2$ kpc [44]. One finds the velocity terminating radius $R_{term} = 52.04$ kpc.

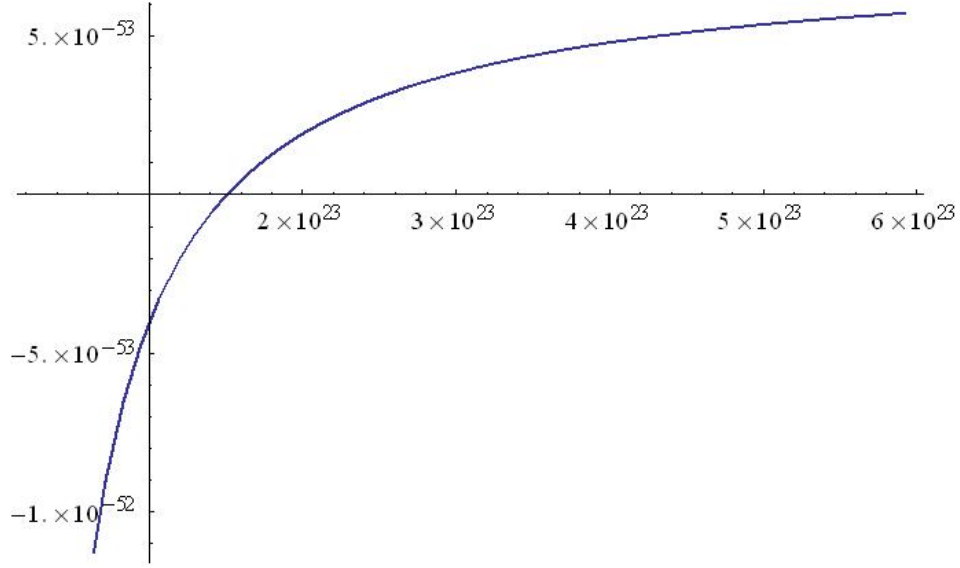


Figure 2: Plot of V'' vs R (cm) using Eq.(21). The crossing shows the halo radius $R_{\text{WR}} = 39.033$ kpc ($\equiv 1.204 \times 10^{23}$ cm), which is the maximally allowed radius supporting stable circular orbits in the halo of ESO 1200211, for which $R_0 = 2$ kpc. The plot is made for the radii $R > 4R_0$.

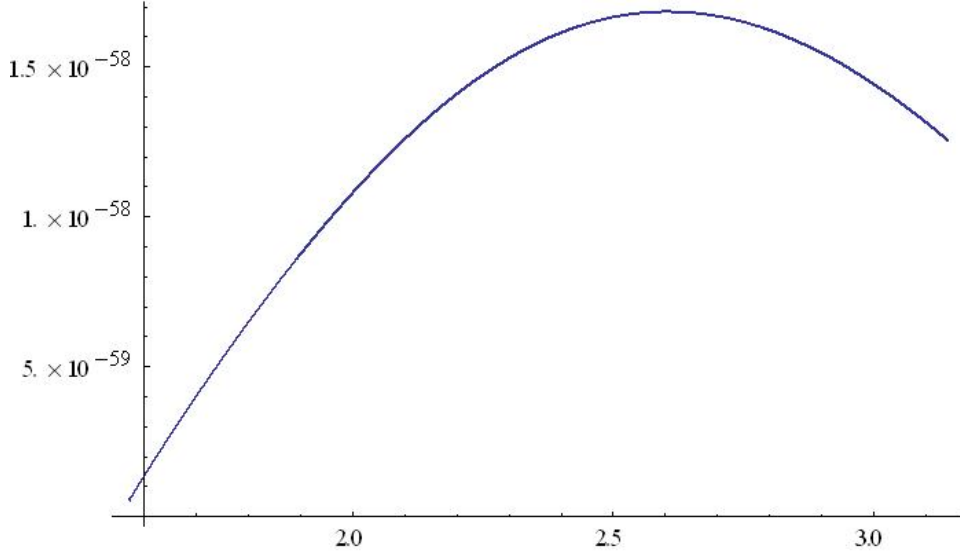


Figure 3: Plot of V'' vs $\bar{R} \in [0.5\pi, \pi]$ using Eq.(30) for ESO 1200211. The chosen parameters are: $r_0 = 0.61$, $v_\infty^2 = 0.000001$, $r_{\text{opt}} = 8$ kpc ($\equiv 2.47 \times 10^{22}$ cm). Here $\rho_0 = 8.25 \times 10^{12} M_\odot \text{kpc}^{-3}$, which corresponds to $\bar{\rho}_0 = 0.50\pi$. The orbits are unstable in the chosen entire radial range $\bar{R} \in [0.5\pi, \pi]$ because $V'' > 0$ there.

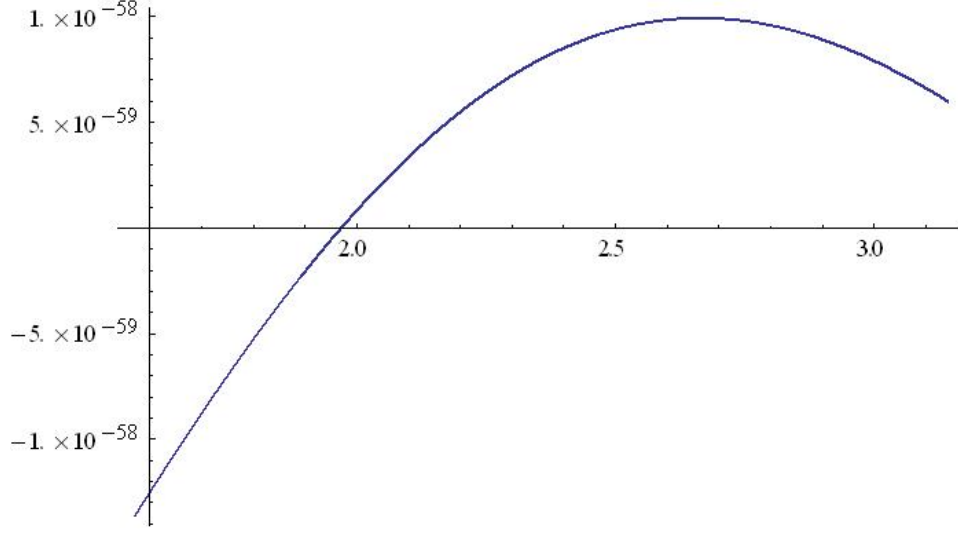


Figure 4: Plot of V'' vs $\bar{R} \in [0.5\pi, \pi]$ using Eq.(30) for ESO 1200211. The chosen parameters are: $r_0 = 0.61$, $v_\infty^2 = 0.000001$, $r_{\text{opt}} = 8$ kpc. Here central density is further lowered to $\rho_0 = 5.61 \times 10^{12} M_\odot \text{kpc}^{-3}$, which corresponds to $\bar{\rho}_0 = 0.34\pi$. The orbit are unstable in some intermediate radii as V'' is partly positive and partly negative.

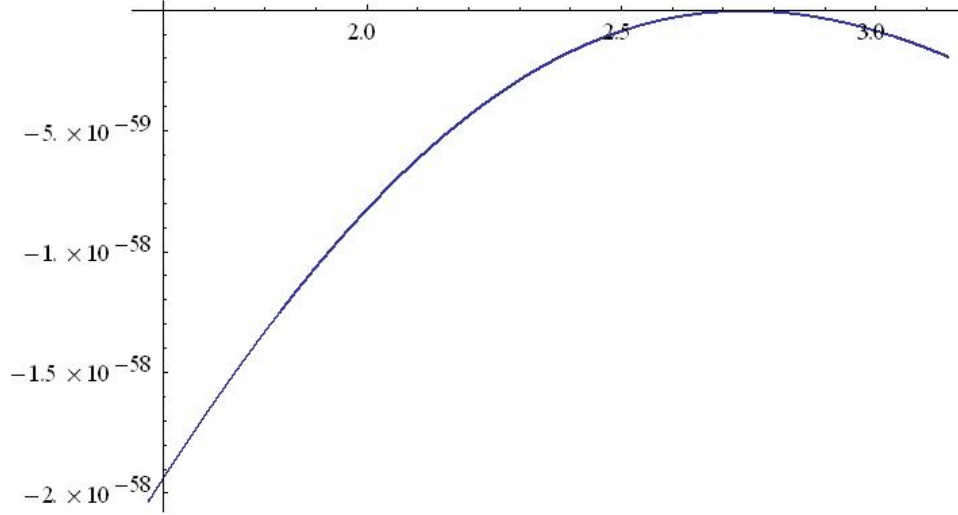


Figure 5: Plot of V'' vs $\bar{R} \in [0.5\pi, \pi]$ using Eq.(30) for ESO 1200211. The chosen parameters are: $r_0 = 0.61$, $v_\infty^2 = 0.000001$, $r_{\text{opt}} = 8$ kpc. Here central density is further lowered to $\rho_0 = 5.04 \times 10^{12} M_\odot \text{kpc}^{-3}$, which corresponds to $\bar{\rho}_0^{\text{upper}} = 0.94 = \beta^{\text{upper}}\pi$, where $\beta^{\text{upper}} = 0.299$. The orbit is *stable* in the entire chosen range for \bar{R} . The corresponding ρ_0 is the upper limit on central density ρ_0^{upper} specific to the sample.

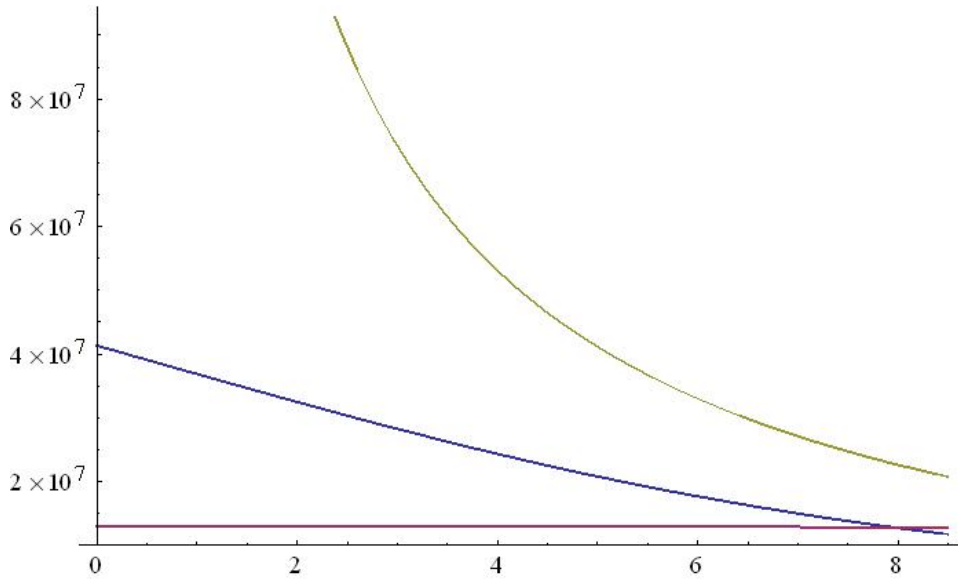


Figure 6: $\rho(r)$ vs r for three profiles for the Milky Way. Bottom brown is BEC profile ($\rho_0^{BEC} = 1.292 \times 10^7 M_\odot \text{kpc}^{-3}$, $\xi = \frac{\pi}{R_{\text{DM}}} = 0.028 \text{ kpc}^{-1}$), Blue curve is Burkert profile ($\rho_0^{BP} = 4.13 \times 10^7 M_\odot \text{kpc}^{-3}$, $r_0 = 9.26 \text{ kpc}$) and the green one is NFW profile ($\rho_0^{NFW} = 1.40 \times 10^7 M_\odot \text{kpc}^{-3}$, $r_S = 16.1 \text{ kpc}$). Uncertainties shown in the original fitted values not considered. Data taken from [132].

Acknowledgments

One of us (Ramil Izmailov) was supported by the Ministry of Education and Science of Russian Federation. This work was supported in part by an internal grant of M. Akmullah Bashkir State Pedagogical University in the field of natural sciences. The authors are thankful to Guzel Kutdusova, Regina Lukmanova and Almir Yanbekov for technical assistance.

REFERENCES

- [1] J. Oort, Some Problems Concerning the Distribution of Luminosities and Peculiar Velocities of Extragalactic Nebulae, *Bull. Astron. Inst. Netherlands* 6 (1931) 155.
- [2] F. Zwicky, Die Rotverschiebung von extragalaktischen Nebeln, *Helv. Phys. Acta* 6 (1933) 110.
- [3] F. Zwicky, On the Masses of Nebulae and of Clusters of Nebulae, *Astrophys. J.* 86 (1937) 217.
- [4] K.C. Freeman, On the Disks of Spiral and so Galaxies, *Astrophys. J.* 160 (1970) 881.
- [5] M.S. Roberts and A.H. Rots, Comparison of Rotation Curves of Different Galaxy Types, *Astron. Astrophys.* 26 (1973) 483.
- [6] P. Ostriker, P.J.E. Peebles and A. Yahill, The size and mass of galaxies, and the mass of the universe, *Astrophys. J. Lett.* 193 (1974) L1.
- [7] J. Einasto, A. Kaasik and E. Saar, Dynamic evidence on massive coronas of galaxies, *Nature* 250 (1974) 309.
- [8] V.C. Rubin, N. Thonnard and W.K. Ford Jr., Extended rotation curves of high-luminosity spiral galaxies. IV. Systematic dynamical properties, Sa through Sc, *Astrophys. J. Lett.* 225 (1978) L107.
- [9] V.C. Rubin, M.S. Roberts and W.K. Ford Jr., Extended rotation curves of high-luminosity spiral galaxies. V. NGC 1961, the most massive spiral known, *Astrophys. J.* 230 (1979) 35.
- [10] Y. Sofue and V. Rubin, Rotation curves of spiral galaxies, *Ann. Rev. Astron. Astrophys.* 39 (2001) 137 [astro-ph/0010594].
- [11] E. Maoz, Gravitational microlensing by dark clusters in the galactic halo, *Astrophys. J.* 428 (1994) L5.
- [12] D.G. Barnes, R.L. Webster, R.W. Schmidt and A. Hughes, Imaging H I in the lensing galaxy 2237 + 0305, *Mon. Not. Roy. Astron. Soc.* 309 (1999) 641.
- [13] Y.-C.N. Cheng and L.M. Krauss, Gravitational lensing and dark structures, *Astrophys. J.* 514 (1999) 25.
- [14] C.M. Trott and R.L. Webster, Dissecting a galaxy: mass distribution of 2237 + 0305, *Mon. Not. Roy. Astron. Soc.* 334 (2002) 621.
- [15] N.N. Weinberg and M. Kamionkowski, Weak gravitational lensing by dark clusters, *Mon. Not. Roy. Astron. Soc.* 337 (2002) 1269.
- [16] R.J. Smith, J.P. Blakeslee, J.R. Lucey and J. Tonry, Discovery of strong lensing by an elliptical galaxy at $z = 0.0345$, *Astrophys. J.* 625 (2005)

L103.

[17] T. Faber and M. Visser, Combining rotation curves and gravitational lensing: How to measure the equation of state of dark matter in the galactic halo, *Mon. Not. Roy. Astron. Soc.* 372 (2006) 136.

[18] R.B. Metcalf and J. Silk, New Constraints on Macroscopic Compact Objects as a Dark Matter Candidate from Gravitational Lensing of Type Ia Supernovae, *Phys. Rev. Lett.* 98 (2007) 071302.

[19] S. Bharadwaj and S. Kar, Modeling galaxy halos using dark matter with pressure, *Phys. Rev. D* 68 (2003) 023516.

[20] M. Colpi, S.L. Shapiro and I. Wasserman, Boson Stars: Gravitational Equilibria of Selfinteracting Scalar Fields, *Phys. Rev. Lett.* 57 (1986) 2485.

[21] G. Efstathiou, W.J. Sutherland and S.J. Maddox, The cosmological constant and cold dark matter, *Nature* 348 (1990) 705.

[22] SDSS collaboration, A.C. Pope et al., Cosmological parameters from Eigenmode analysis of Sloan Digital Sky Survey galaxy redshifts, *Astrophys. J.* 607 (2004) 655.

[23] SDSS collaboration, M. Tegmark et al., Cosmological parameters from SDSS and WMAP, *Phys. Rev. D* 69 (2004) 103501.

[24] SDSS collaboration, M. Tegmark et al., The three-dimensional power spectrum of galaxies from the SDSS, *Astrophys. J.* 606 (2004) 702.

[25] T. Matos, F.S. Guzman and D. Nunez, Spherical scalar field halo in galaxies, *Phys. Rev. D* 62 (2000) 061301.

[26] P.J.E. Peebles, Dynamics of a dark matter field with a quartic self-interaction potential, *Phys. Rev. D* 62 (2000) 023502.

[27] T. Matos and F.S. Guzman, Scalar fields as dark matter in spiral galaxies, *Class. Quant. Grav.* 17 (2000) L9 [gr-qc/9810028].

[28] U. Nucamendi, M. Salgado and D. Sudarsky, An Alternative approach to the galactic dark matter problem, *Phys. Rev. D* 63 (2001) 125016 [gr-qc/0011049].

[29] E.W. Mielke and F.E. Schunck, Nontopological scalar soliton as dark matter halo, *Phys. Rev. D* 66 (2002) 023503.

[30] L.G. Cabral-Rosetti, T. Matos, D. Nunez and R.A. Sussman, Hydrodynamics of galactic dark matter, *Class. Quant. Grav.* 19 (2002) 3603 [gr-qc/0112044].

[31] J.E. Lidsey, T. Matos and L.A. Urena-Lopez, The Inflaton field as selfinteracting dark matter in the brane world scenario, *Phys. Rev. D* 66 (2002) 023514.

[32] A. Arbey, J. Lesgourgues and P. Salati, Galactic halos of fluid dark matter, *Phys. Rev. D* 68 (2003) 023511.

[33] M.K. Mak and T. Harko, Can the galactic rotation curves be explained in brane world models?, *Phys. Rev. D* 70 (2004) 024010 [gr-qc/0404104].

- [34] A. Borriello and P. Salucci, The Dark matter distribution in disk galaxies, *Mon. Not. Roy. Astron. Soc.* 323 (2001) 285.
- [35] P.D. Mannheim, Alternatives to dark matter and dark energy, *Prog. Pari. Nucl. Phys.* 56 (2006) 340.
- [36] M. Milgrom, A Modification of the Newtonian dynamics as a possible alternative to the hidden mass hypothesis, *Astrophys. J.* 270 (1983) 365.
- [37] M. Milgrom, A Modification of the Newtonian dynamics: Implications for galaxies, *Astrophys. J.* 270 (1983) 371.
- [38] M. Milgrom, A modification of the Newtonian dynamics: implications for galaxy systems, *Astrophys. J.* 270 (1983) 384.
- [39] R.H. Sanders, The published extended rotation curves of spiral galaxies: confrontation with modified dynamics, *Astrophys. J.* 473 (1996) 117.
- [40] R.A. Swaters, R.H. Sanders and S.S. McGaugh, Testing Modified Newtonian Dynamics with Rotation Curves of Dwarf and Low Surface Brightness Galaxies, *Astrophys. J.* 718 (2010) 380 [arXiv:1005.5456].
- [41] G. Gentile, B. Famaey, F. Combes, P. Kroupa, H.S. Zhao and O. Tiret, Tidal dwarf galaxies as a test of fundamental physics, *Astron. Astrophys.* 472 (2007) L25 [arXiv:0706.1976].
- [42] L. Iorio, Galactic Sun's motion in the cold dark matter, Modified Newtonian Dynamics and modified gravity scenarios, *Astron. Nachr.* 330 (2009) 857.
- [43] J.W. Moffat, Scalar-tensor-vector gravity theory, *JCAP* 03 (2006) 004 [gr-qc/0506021].
- [44] J.R. Brownstein and J.W. Moffat, Galaxy rotation curves without non-baryonic dark matter, *Astrophys. J.* 636 (2006) 721.
- [45] S. Capozziello, V.F. Cardone and A. Troisi, Low surface brightness galaxies rotation curves in the low energy limit of R_n gravity: no need for dark matter?, *Mon. Not. Roy. Astron. Soc.* 375 (2007) 1423.
- [46] E.E. Flanagan, Fourth order Weyl gravity, *Phys. Rev. D* 74 (2006) 023002.
- [47] P.D. Mannheim, Schwarzschild limit of conformal gravity in the presence of macroscopic scalar fields, *Phys. Rev. D* 75 (2007) 124006 [gr-qc/0703037].
- [48] P.D. Mannheim and J.G. O'Brien, Impact of a global quadratic potential on galactic rotation curves, *Phys. Rev. Lett.* 106 (2011) 121101 [arXiv:1007.0970].
- [49] G.R. Blumenthal, S.M. Faber, J.R. Primack and M.J. Rees, Formation of Galaxies and Large Scale Structure with Cold Dark Matter, *Nature* 311 (1984) 517.
- [50] A.R. Liddle and D.H. Lyth, The Cold dark matter density perturbation, *Phys. Rept.* 231 (1993).
- [51] P.J.E. Peebles, Large scale background temperature and mass fluctuations due to scale invariant primeval perturbations, *Astrophys. J.* 263

(1982) L1.

[52] P.J.E. Peebles, Dark matter and the origin of galaxies and globular star clusters, *Astrophys. J.* 277 (1984) 470.

[53] S. Basilakos and J.A.S. Lima, Constraints on Cold Dark Matter Accelerating Cosmologies and Cluster Formation, *Phys. Rev. D* 82 (2010) 023504 [arXiv:1003.5754].

[54] S. McGaugh, Dynamics and the second peak: Cold dark matter?, *Int. J. Mod. Phys. A* 16S1C (2001) 1031.

[55] C.S. Kochanek, E.E. Falco, C. Impey, J. Lehar, B. McLeod and H.-W. Rix, CASTLE Survey Gravitational Lens Data Base (2005).

[56] V.K. Onemli, Probing Cold Dark Matter Cusps by Gravitational Lensing, *Int. J. Mod. Phys. D* 15 (2006) 2059.

[57] S. Dodelson, E.I. Gates and M.S. Turner, Cold dark matter models, *Science* 274 (1996) 69.

[58] J.-c. Hwang and H. Noh, Axion as a Cold Dark Matter candidate, *Phys. Lett. B* 680 (2009) 1 [arXiv:0902.4738].

[59] S.L. Dubovsky, P.G. Tinyakov and I.I. Tkachev, Massive graviton as a testable cold dark matter candidate, *Phys. Rev. Lett.* 94 (2005) 181102.

[60] C. Evoli, A. Mesinger and A. Ferrara, Unveiling the nature of dark matter with high redshift 21 cm line experiments, *JCAP* 11 (2014) 024 [arXiv:1408.1109].

[61] O.F. Piattella, D.L.A. Martins and L. Casarini, Sub-horizon evolution of cold dark matter perturbations through dark matter-dark energy equivalence epoch, *JCAP* 10 (2014) 031 [arXiv:1407.4773].

[62] C.M. Ho, D. Minic and Y.J. Ng, Cold Dark Matter with MOND Scaling, *Phys. Lett. B* 693 (2010) 567 [arXiv:1005.3537].

[63] C. Rampf and G. Rigopoulos, Initial conditions for cold dark matter particles and General Relativity, *Phys. Rev. D* 87 (2013) 123525 [arXiv:1305.0010].

[64] A.A. Grib and Y. Pavlov, Cold dark matter and primordial super-heavy particles, *Int. J. Mod. Phys. A* 17 (2002) 4435 [gr-qc/0211015].

[65] A. Zhitnitsky, Cold dark matter as compact composite objects, *Phys. Rev. D* 74 (2006) 043515.

[66] H. Li, J. Liu, J.-Q. Xia and Y.-F. Cai, Cold Dark Matter Isocurvature Perturbations: Cosmological Constraints and Applications, *Phys. Rev. D* 83 (2011) 123517 [arXiv:1012.2511].

[67] AMS collaboration, M. Aguilar et al., First Result from the Alpha Magnetic Spectrometer on the International Space Station: Precision Measurement of the Positron Fraction in Primary Cosmic Rays of 0.5-350 GeV, *Phys. Rev. Lett.* 110 (2013) 141102.

[68] A. De Simone, A. Riotto and W. Xue, Interpretation of AMS-02 Results: Correlations among Dark Matter Signals, *JCAP* 05 (2013) 003 [arXiv:1304.1336].

- [69] J. Binney and S. Tremaine, Galactic dynamics, Princeton University Press, Princeton U.S.A.(1987).
- [70] M. Persic, P. Salucci and F. Stel, The Universal rotation curve of spiral galaxies: 1. The Dark matter connection, *Mon. Not. Roy. Astron. Soc.* 281 (1996) 27.
- [71] H.J. de Vega, P. Salucci and N.G. Sanchez, The mass of the dark matter particle from theory and observations, *New Astron.* 17 (2012) 653 [arXiv:1004.1908].
- [72] S. Nojiri and S.D. Odintsov, Gravity assisted dark energy dominance and cosmic acceleration, *Phys. Lett. B* 599 (2004) 137.
- [73] G. Allemandi, A. Borowiec, M. Francaviglia and S.D. Odintsov, Dark energy dominance and cosmic acceleration in first order formalism, *Phys. Rev. D* 72 (2005) 063505 [gr-qc/0504057].
- [74] S. Nojiri and S.D. Odintsov, Unified cosmic history in modified gravity: from F(R) theory to Lorentz non-invariant models, *Phys. Rept.* 505 (2011) 59 [arXiv:1011.0544].
- [75] O. Bertolami, C.G. Boehmer, T. Harko and F.S.N. Lobo, Extra force in f (R) modified theories of gravity, *Phys. Rev. D* 75 (2007) 104016 [arXiv:0704.1733].
- [76] T. Harko and F.S.N. Lobo, f (R, Lm) gravity, *Eur. Phys. J. C* 70 (2010) 373 [arXiv:1008.4193].
- [77] T. Delsate and J. Steinhoff, New insights on the matter-gravity coupling paradigm, *Phys. Rev. Lett.* 109 (2012) 021101 [arXiv:1201.4989].
- [78] M. Baiados and P.G. Ferreira, Eddington's theory of gravity and its progeny, *Phys. Rev. Lett.* 105 (2010) 011101 [arXiv:1006.1769].
- [79] S. Deser and G.W. Gibbons, Born-Infeld-Einstein actions?, *Class. Quant. Grav.* 15 (1998) L35.
- [80] J. Casanellas, P. Pani, I. Lopes and V. Cardoso, Testing alternative theories of gravity using the Sun, *Astrophys. J.* 745 (2012) 15 [arXiv:1109.0249].
- [81] P. Pani, V. Cardoso and T. Delsate, Compact stars in Eddington inspired gravity, *Phys. Rev. Lett.* 107 (2011) 031101 [arXiv:1106.3569].
- [82] T. Harko, F.S.N. Lobo, M.K. Mak and S.V. Sushkov, Structure of neutron, quark and exotic stars in Eddington-inspired Born-Infeld gravity, *Phys. Rev. D* 88 (2013) 044032 [arXiv:1305.6770].
- [83] J.H.C. Scargill, M. Banados and P.G. Ferreira, Cosmology with Eddington-inspired Gravity, *Phys. Rev. D* 86 (2012) 103533 [arXiv:1210.1521].
- [84] P.P. Avelino and R.Z. Ferreira, Bouncing Eddington-inspired Born-Infeld cosmologies: an alternative to Inflation?, *Phys. Rev. D* 86 (2012) 041501 [arXiv:1205.6676].
- [85] X.-L. Du, K. Yang, X.-H. Meng and Y.-X. Liu, Large Scale Structure Formation in Eddington-inspired Born-Infeld Gravity, *Phys. Rev. D* 90 (2014) 044054 [arXiv:1403.0083].

- [86] Y.-X. Liu, K. Yang, H. Guo and Y. Zhong, Domain Wall Brane in Eddington Inspired Born-Infeld Gravity, *Phys. Rev. D* 85 (2012) 124053 [arXiv:1203.2349].
- [87] Q.-M. Fu, L. Zhao, K. Yang, B.-M. Gu and Y.-X. Liu, Stability and (quasi)localization of gravitational fluctuations in an Eddington-inspired Born-Infeld brane system, *Phys. Rev. D* 90 (2014) 104007 [arXiv:1407.6107].
- [88] S.-W. Wei, K. Yang and Y.-X. Liu, Black hole solution and strong gravitational lensing in Eddington-inspired Born-Infeld gravity, *Eur. Phys. J. C* 75 (2015) 253 [arXiv:1405.2178].
- [89] A. Edery and M.B. Paranjape, Classical tests for Weyl gravity: Deflection of light and radar echo delay, *Phys. Rev. D* 58 (1998) 024011.
- [90] A. Bhattacharya, A. Panchenko, M. Scalia, C. Cattani and K.K. Nandi, Light bending in the galactic halo by Rindler-Ishak method, *JCAP* 09 (2010) 004 [arXiv:0910.1112].
- [91] A. Bhattacharya, G.M. Garipova, E. Laserra, A. Bhadra and K.K. Nandi, The Vacuole Model: New Terms in the Second Order Deflection of Light, *JCAP* 02 (2011) 028 [arXiv:1002.2601].
- [92] D. Cutajar and K.Z. Adami, Strong lensing as a test for Conformal Weyl Gravity, *Mon. Not. Roy. Astron. Soc.* 441 (2014) 1291 [arXiv:1403.7930].
- [93] F. Rahaman, K.K. Nandi, A. Bhadra, M. Kalam and K. Chakraborty, Perfect Fluid Dark Matter, *Phys. Lett. B* 694 (2010) 10 [arXiv:1009.3572].
- [94] T. Harko and F.S.N. Lobo, Two-fluid dark matter models, *Phys. Rev. D* 83 (2011) 124051 [arXiv:1106.2642].
- [95] T. Harko, F.S.N. Lobo, M.K. Mak and S.V. Sushkov, Dark matter density profile and galactic metric in Eddington-inspired Born-Infeld gravity, *Mod. Phys. Lett. A* 29 (2014) 1450049.
- [96] P. Pani, T. Delsate and V. Cardoso, Eddington-inspired Born-Infeld gravity. Phenomenology of non-linear gravity-matter coupling, *Phys. Rev. D* 85 (2012) 084020 [arXiv:1201.2814].
- [97] P. Salucci and A. Burkert, Dark matter scaling relations, *Astrophys. J.* 537 (2000) L9.
- [98] P. Salucci and M. Persic, Maximal halos in high-luminosity spiral galaxies, *Astron. Astrophys.* 351 (1999) 442.
- [99] K.K. Nandi, A.I. Filippov, F. Rahaman, S. Ray, A.A. Usmani et al., Features of galactic halo in a brane world model and observational constraints, *Mon. Not. Roy. Astron. Soc.* 399 (2009) 2079 [arXiv:0812.2545].
- [100] K.K. Nandi and A. Bhadra, Comment on 'Impact of a Global Quadratic Potential on Galactic Rotation Curves', *Phys. Rev. Lett.* 109 (2012) 079001 [arXiv:1208.5330].
- [101] K. Lake, Galactic potentials, *Phys. Rev. Lett.* 92 (2004) 051101 [gr-qc/0302067].
- [102] D.N. Vollick, Palatini approach to Born-Infeld-Einstein theory and a geometric description of electrodynamics, *Phys. Rev. D* 69 (2004) 064030

[gr-qc/0309101].

[103] D.N. Vollick, Born-Infeld-Einstein theory with matter, *Phys. Rev. D* 72 (2005) 084026 [gr-qc/0506091].

[104] W.J.G. de Blok, S.S. McGaugh, A. Bosma and V.C. Rubin, Mass density profiles of LSB galaxies, *Astrophys. J.* 552 (2001) L23.

[105] S. Chandrasekhar, *Mathematical Theory of Black Holes*, Oxford University Press, Oxford U.K. (1983).

[106] P.D. Mannheim and D. Kazanas, Exact Vacuum Solution to Conformal Weyl Gravity and Galactic Rotation Curves, *Astrophys. J.* 342 (1989) 635.

[107] P.D. Mannheim and J.G. O'Brien, Fitting galactic rotation curves with conformal gravity and a global quadratic potential, *Phys. Rev. D* 85 (2012) 124020 [arXiv:1011.3495].

[108] V.H. Robles and T. Matos, Flat Central Density Profile and Constant DM Surface Density in Galaxies from Scalar Field Dark Matter, *Mon. Not. Roy. Astron. Soc.* 422 (2012) 282 [arXiv:1201.3032].

[109] R.H. Sanders, The published extended rotation curves of spiral galaxies: confrontation with modified dynamics, *Astrophys. J.* 473 (1996) 117 [astro-ph/9606089].

[110] D. Lynden-Bell and G. Gilmore eds., *Baryonic Dark Matter*, Kluwer, Dordrecht Netherlands (1990).

[111] K. Kuijken and G. Gilmore, The mass distribution in the galactic disc I. A technique to determine the integral surface mass density of the disc near the Sun, *Mon. Not. Roy. Astron. Soc.* 239 (1989) 571.

[112] K. Kuijken and G. Gilmore, The Mass Distribution in the Galactic Disc II. Determination of the Surface Mass Density of the Galactic Disc Near the Sun, *Mon. Not. Roy. Astron. Soc.* 239 (1989) 605 .

[113] K. Kuijken and G. Gilmore, The mass distribution in the galactic disc III. The local volume mass density, *Mon. Not. Roy. Astron. Soc.* 239 (1989) 651.

[114] K. Kuijken and G. Gilmore, The galactic disk surface mass density and the Galactic force $K(z)$ at $Z = 1.1$ kiloparsecs, *Astrophys. J.* 367 (1991) L9.

[115] W.J.G. de Blok and S.S. McGaugh, The Dark and visible matter content of low surface brightness disk galaxies, *Mon. Not. Roy. Astron. Soc.* 290 (1997) 533.

[116] A. Burkert, The structure of dark matter halos in dwarf galaxies, *Astrophys. J.* 447 (1995) L25.

[117] P. Salucci, A. Lapi, C. Tonini, G. Gentile, I. Yegorova and U. Klein, The Universal Rotation Curve of Spiral Galaxies II. The Dark Matter Distribution out to the Virial Radius, *Mon. Not. Roy. Astron. Soc.* 378 (2007) 41.

[118] S. Grossman and R. Narayan, Gravitationally lensed images in Abell 370, *Astrophys. J.* 344(1989) 637.

- [119] M. Bartelmann and R. Narayan, Gravitational lensing and the mass distribution of clusters, *AIP Conf. Proc.* 336 (1995) 307.
- [120] K.G. Begeman, A.H. Broeils and R.H. Sanders, Extended rotation curves of spiral galaxies: Dark haloes and modified dynamics, *Mon. Not. Roy. Astron. Soc.* 249 (1991) 523.
- [121] J.F. Navarro, C.S. Frenk and S.D.M. White, The Structure of cold dark matter halos, *Astrophys. J.* 462 (1996) 563.
- [122] J.F. Navarro, C.S. Frenk and S.D.M. White, A Universal density profile from hierarchical clustering, *Astrophys. J.* 490 (1997) 493.
- [123] P.R. Kafle, S. Sharma, G.F. Lewis and J. Bland-Hawthorn, On the Shoulders of Giants: Properties of the Stellar Halo and the Milky Way Mass Distribution, *Astrophys. J.* 794 (2014) 59 [arXiv:1408.1787].
- [124] S.M. Faber and J.S. Gallagher, Masses and mass-to-light ratios of galaxies, *Ann. Rev. Astron. Astrophys.* 17 (1979) 135.
- [125] P.J. McMillan, Mass models of the Milky Way, *Mon. Not. Roy. Astron. Soc.* 414 (2011) 2446 [arXiv:1102.4340].
- [126] F. Iocco, M. Pato, G. Bertone and P. Jetzer, Dark Matter distribution in the Milky Way: microlensing and dynamical constraints, *JCAP* 11 (2011) 029 [arXiv:1107.5810].
- [127] A.J. Deason, V. Belokurov, N.W. Evans and J.H. An, Broken Degeneracies: The Rotation Curve and Velocity Anisotropy of the Milky Way Halo, *Mon. Not. Roy. Astron. Soc.* 424 (2012) L44 [arXiv:1204.5189].
- [128] A.J. Deason, V. Belokurov, N.W. Evans, S.E. Koposov, R.J. Cooke et al., The cold veil of the Milky Way stellar halo, *Mon. Not. Roy. Astron. Soc.* 425 (2012) 2840 [arXiv:1205.6203]. [129] L.E. Strigari, Galactic Searches for Dark Matter, *Phys. Rept.* 531 (2013) 1 [arXiv:1211.7090].
- [130] G. Bertone, D. Hooper and J. Silk, Particle dark matter: Evidence, candidates and constraints, *Phys. Rept.* 405 (2005) 279.
- [131] J.I. Read, The Local Dark Matter Density, *J. Phys. G* 41 (2014) 063101 [arXiv:1404.1938].
- [132] F. Nesti and P. Salucci, The Dark Matter halo of the Milky Way, *AD 2013, JCAP* 07 (2013) 016 [arXiv:1304.5127].
- [133] J.N. Bahcall, M. Schmidt and R.M. Soneira, The Galactic Spheroid, *Astrophys. J.* 265 (1983) 730.
- [134] J.A.R. Caldwell and J.P. Ostriker, The Mass distribution within our Galaxy: A Three component model, *Astrophys. J.* 251 (1981) 61.
- [135] M.S. Turner, Cosmic and Local Mass Density of Invisible Axions, *Phys. Rev. D* 33 (1986) 889.
- [136] G. Jungman, M. Kamionkowski and K. Griest, Supersymmetric dark matter, *Phys. Rept.* 267 (1996) 195.
- [137] J. Bovy and S. Tremaine, On the local dark matter density, *Astrophys. J.* 756 (2012) 89 [arXiv:1205.4033].
- [138] L. Bergstrom, P. Ullio and J.H. Buckley, Observability of gamma-rays from dark matter neutralino annihilations in the Milky Way halo, *As-*

tropart. Phys. 9 (1998) 137.

[139] M. Pato, O. Agertz, G. Bertone, B. Moore and R. Teyssier, Systematic uncertainties in the determination of the local dark matter density, Phys. Rev. D 82 (2010) 023531 [arXiv:1006.1322].

[140] W.J.G. de Blok, S.S. McGaugh and V.C. Rubin, High-Resolution Rotation Curves of Low Surface Brightness Galaxies. II. Mass Models, Astron. J. 122 (2001) 2396.

[141] P. Salucci and M. Persic, The Baryonic mass function of spiral galaxies: Clues to galaxy formation and to the nature of damped Lyman alpha clouds, Mon. Not. Roy. Astron. Soc. 309 (1999) 923.

[142] L. Iorio, Effect of Sun and Planet-Bound Dark Matter on Planet and Satellite Dynamics in the Solar System, JCAP 05 (2010) 018 [arXiv:1001.1697].

[143] G. Battaglia, A. Helmi, H. Morrison, P. Harding, E.W. Olszewski et al., The Radial velocity dispersion profile of the Galactic Halo: Constraining the density profile of the dark halo of the Milky Way, Mon. Not. Roy. Astron. Soc. 364 (2005) 433.

[144] M.I. Wilkinson and N.W. Evans, The present and future mass of the Milky Way halo, Mon. Not. Roy. Astron. Soc. 310 (1999) 645.